HIV-1 Vpr antagonizes cGAS sensing by targeting karyopherin-mediated NF-κB/IRF3 nuclear transport

Hataf Khan[1,2,+], Rebecca P. Sumner[1,+], Jane Rasaiyaah[1,3], Choon Ping Tan[1,4], Maria Teresa Rodriguez-Plata[1,5], Chris van Tulleken[1], Douglas Fink[1], Lorena Zuliani-Alvarez[1], Lucy Thorne[1], David Stirling[1,6] & Greg J. Towers[1]

[1]Division of Infection and Immunity, University College London, 90 Gower Street, London, UK
[2]Current address: Department of Infectious Diseases, King's College London, London, UK
[3]Current address: Molecular and Cellular Immunology Unit, UCL Great Ormond Street Institute of Child Health, London, UK.
[4]Current address: Translation & Innovation Hub, 80 Wood Lane, London, UK
[5]Current address: Black Belt TX Ltd, Stevenage Bioscience Catalyst, Gunnels Wood Rd, Stevenage, UK
[6]Current address: Broad Institute of MIT and Harvard University, Cambridge, MA, USA.
[+]equal contribution
*Correspondence: g.towers@ucl.ac.uk

Summary (150 words)

HIV-1 must replicate in cells that are equipped to defend themselves from infection through the intracellular innate immune system. Hence, HIV-1 evades innate immune sensing through encapsidated DNA synthesis and encodes accessory genes that antagonize specific antiviral effectors. Here we show that the HIV-1 Vpr protein antagonizes the stimulatory effect of a variety of pathogen associated molecular patterns, including cytoplasmic DNA, by inhibiting IRF3 and NF-κB nuclear transport. Both particle associated, and expressed Vpr, antagonized innate immune signaling. Phosphorylation of IRF3 at S396, but not S386, was also inhibited by Vpr. We provide evidence that Vpr interacts with karyopherins and disturbs their recruitment of IRF3 and NF-κB to prevent nuclear transport. Our data demonstrate Vpr rescue of HIV-1 replication in human macrophages from inhibition by cGAMP, the product of activated cGAS. We propose that Vpr inhibition of innate immune activation serves a critical function in promoting HIV-1 replication and transmission.

Key words: HIV-1, Vpr, DNA sensing, cGAS, Karyopherin, IRF3, NF- κB, nuclear transport

Introduction

Like all viruses, lentiviruses must navigate the hostile environment of the host cell in order to infect, produce new viral particles, and transmit to new cells. A principal feature of cellular defences is detection or sensing of incoming viruses and subsequent production of inflammatory cytokines, particularly type 1 interferons (IFNs). All viral infections likely trigger IFN *in vivo* and the degree to which they do this, and their capacity to antagonize IFN activity and its complex effects, are key in determining transmission mechanism, host range and disease pathogenesis. Like other viruses, lentiviruses antagonize specific host proteins or pathways that would otherwise suppress infection. For example, HIV-1 antagonizes IFN induced restriction factors through accessory genes encoding Vif (APOBEC3G/H), Vpu (tetherin) and Nef (tetherin/SERINC3/5) (Foster et al., 2017; Sumner et al., 2017) Although Vpr has been implicated in manipulating host defences to facilitate replication, its mechanisms and its innate immune relevant target proteins have been obscure (Trotard et al., 2016). This is partly because demonstration of Vpr-dependent HIV-1 replication has been elusive and results inconsistent between studies (Dedera et al., 1989; Fouchier et al., 1998; Hattori et al., 1990). Vpr clearly changes infected cell protein profiles changing the level of hundreds of proteins in proteomic studies, probably indirectly in most cases (Greenwood et al., 2019). There is also evidence for Vpr interacting directly with particular proteins such as its cofactor DCAF1 (Zhang et al., 2001), the host enzyme UNG2 (Wu et al., 2016) as well as HTLF (Lahouassa et al., 2016; Yan et al., 2019), SLX4 (Laguette et al., 2014) and CCDC137 (Zhang & Bieniasz, 2019). However, the mechanistic details of Vpr promotion of HIV replication are poorly understood.

Here we show that Vpr rescues HIV-1 replication in innate immune activated macrophages. We show that Vpr suppresses nuclear entry of the activated inflammatory transcription factors IRF3 and NF-κB. We identify Vpr mutants that fail to recruit to the nuclear envelope, and fail to antagonize innate sensing, but retain induction of cell cycle arrest, genetically separating key Vpr functions. We also provide evidence that wild type (WT) Vpr, but not functionally inactive Vpr mutants, prevent IRF3 and NF-κB nuclear transport by recruiting karyopherin alpha 1 (KPNA1) and competing with IRF3 and NF-κB p65, for KPNA1 mediated nuclear import.

Results

HIV-1 replication in cGAMP-stimulated MDMs requires Vpr

We prepared human monocyte-derived macrophages (MDM) by purifying monocytes from peripheral blood by adherence and treating with M-CSF (Rasaiyaah et al., 2013). Macrophages prepared in this way are particularly permissive to HIV-1 replication facilitating study of HIV-1 biology in a primary myeloid cell type. In MDM, wild type HIV-1 and HIV-1ΔVpr replicated equally well, measuring infection by staining infected cells with anti-Gag antibody (Figure 1A) (Rasaiyaah et al., 2013) as has been previously shown (Fouchier et al., 1998). Wild type and ΔVpr virus also

77 replicated equally well in activated CD4+ T cells purified from peripheral blood, consistent with
78 previous studies (Figure S1A) (Dedera et al., 1989; Fouchier et al., 1998). We hypothesized that,
79 given HIV synthesizes a DNA pathogen associated molecular pattern (PAMP) in the cytoplasm,
80 then Vpr might be particularly important when DNA sensing is activated. In fact, mimicking
81 activation of DNA sensor cGAS by treating cells with cGAMP, the product of activated cGAS,
82 induced Vpr-dependent HIV-1 replication in MDM. 1μg/ml cGAMP specifically suppressed HIV-
83 1ΔVpr more potently than wild type virus and 4μg/ml cGAMP overcame Vpr activity and
84 suppressed replication of both wild type and mutant viruses (Figure 1A). Intriguingly, Vpr did not
85 rescue HIV-1 replication from cGAMP-mediated inhibition in primary human CD4+ T cells, and
86 cGAMP treatment did not particularly inhibit replication in a Jurkat T cell line, suggesting that the
87 consequences of cGAMP treatment differ between macrophages and T cells (Figure S1A)
88 consistent with previous observations (Gulen et al., 2017; Xu et al., 2016).
89
90 **HIV-1 particle delivered Vpr inhibits gene expression stimulated by DNA sensing**
91 We next tested Vpr activity in THP-1 cells, a tractable cell line for studying myeloid cell biology.
92 THP-1 naturally express cGAS and STING and have a functional DNA sensing pathway
93 (Mankan et al., 2014). THP-1 cells expressing the Gaussia luciferase gene under the control of
94 the endogenous promoter for the *IFIT1* gene (herein referred to as THP-1 IFIT1-luc) have been
95 described (Mankan et al., 2014) and were used to study the effect of virion-associated Vpr on
96 cGAMP activation of IFIT1-luc expression. IFIT1, (ISG56), is a well-characterized ISG that is
97 highly sensitive to cGAMP and type 1 IFN.
98
99 Treatment of THP-1 IFIT-luc cells with cGAMP induced IFIT1-luc expression by two orders of
100 magnitude (Figure 1B). THP-1 were then infected with VSV-G pseudotyped HIV-1 GFP and
101 simultaneously stimulated with 5μg/ml cGAMP and luciferase was read at 6 hours, 8 hours and
102 24 hours post-infection (Figure 1B). Consistent with data in MDM, infection with VSV-G
103 pseudotyped HIV-1, genome-free, particles bearing Vpr, (referred to here as virus-like particles
104 or VLP), but not VLP lacking Vpr, suppressed IFIT1-luc induction by over an order of magnitude
105 (Figure 1B). Doses of VLP required to suppress IFIT1-luc expression were high, equivalent to a
106 multiplicity of infection of 20 as measured by correlating VLP reverse transcriptase levels (SG-
107 PERT) (Vermeire et al., 2012), with HIV-1 GFP titers. We assume that such a high dose is
108 required because cGAMP treatment activates numerous STING complexes in most of the
109 cGAMP-treated cells. Therefore, correspondingly large doses of Vpr-bearing VLP are required to
110 suppress activation. Conversely, if cGAS/STING is activated by a high dose of the HIV particles
111 themselves, which only contain a single DNA genome molecule, we expect that the amount of
112 Vpr contained in an individual particle should be sufficient to suppress activation. To test this, we
113 activated DNA sensing using high dose infection by VSV-G pseudotyped HIV-1 vectors bearing
114 GFP-encoding genome. We used an HIV-1 packaging plasmid, derived from HIV-1 clone R9,

115 encoding Gag-Pol, Tat and Rev (p8.91) or Gag-Pol, Tat and Rev and Vpr, Vpu, Vif and Nef
116 (p8.2) (Zufferey et al., 1997). We infected THP-1 cells with similar doses of HIV-1 GFP, prepared
117 using p8.2 and therefore bearing Vpr, or p8.91 with no Vpr. Strikingly, although Vpr positive and
118 negative HIV-1 GFP stocks infected the THP-1 to similar levels (Figure 1D), induction of
119 inflammatory cytokine and ISG CXCL10 was reduced if the HIV-1 GFP carried Vpr (p8.2) (Figure
120 1C). This indicates that although sensing is activated, this does not reduce the infectivity of
121 single round HIV-1 GFP vector infectivity. A role for sensing of viral DNA was evidenced by our
122 observation that HIV-1 particles made without genome did not induce CXCL10 expression (Fig
123 1E). In this experiment, p8.91 derived HIV-1 GFP, bearing genome, but not Vpr, acted as a
124 positive control and activated CXCL10 expression as before. HIV-1 GFP bearing Vpr did not
125 activate CXCL10 expression, as before (Figure 1C, E). Infection by HIV-1 particles without
126 genome were uninfectious while Vpr+ and Vpr- HIV-1 GFP particles containing viral DNA were
127 equally infectious (Figure 1F). Induction of CXCL10 expression induced by HIV-1 GFP was
128 dependent on cGAS because THP-1 cGAS knock out cells did not induce CXCL10, whereas
129 knock out of the RNA sensing adaptor protein MAVS had no effect (Figure 1G). Importantly,
130 single round titer of HIV-1 GFP was not affected by cGAS or MAVS knock out, confirming that
131 sensing activation does not impact single round infectivity of HIV-1 GFP VSV-G pseudotypes in
132 this assay (Figure 1H, Figure S1B). cGAS and MAVS knockout were confirmed by immunoblot
133 (Figure S1C).
134
135 **HIV-1 Vpr expression inhibits interferon stimulated gene expression after DNA sensing**
136 We next tested whether Vpr expression can suppress innate immune activation by cGAMP using
137 THP-1 IFIT1-luc cells. Vpr from the primary founder HIV-1 clone SUMA (Fischer et al., 2010) was
138 expressed using the HIV-1 vector pCSVIG (Figure S2A, S2B) titrating between an MOI of
139 approximately 0.2-1. Cells were then treated with cGAMP (5µg/ml) 40 hours after infection with
140 Vpr encoding vector, and IFIT1-luc was measured 8 hours after cGAMP treatment.
141 Untransduced cells expressed IFIT1-luc readily on cGAMP stimulation, as did cells infected with
142 empty vector (Figure 2A). However, prior expression of Vpr reduced IFIT1-luc responses in a
143 dose-dependent manner. The highest doses of Vpr encoding vector, corresponding to an MOI of
144 about 1, suppressed IFIT1-luc expression by an order of magnitude (Figure 2A). Importantly,
145 expression of empty vector at the highest dose (MOI=1) did not reduce IFIT1-luc induction by
146 cGAMP (Figure 2A). Vpr expression (MOI=1, Figure S2C) also suppressed cGAMP-mediated
147 induction of endogenous ISG mRNA expression, measured by qRT-PCR for *MxA*, *CXCL10*,
148 *IFIT2* and *viperin* (Figure 2B). In a separate experiment, secreted CXCL10, induced by cGAMP
149 treatment of THP-1, was also inhibited by Vpr expression (Figure 2C), (infection data in Figure
150 S2D). Consistent with the notion that Vpr antagonizes DNA sensing, IFIT1-luc expression
151 stimulated by transfection of Herring Testis (HT) DNA was also inhibited by Vpr expression in
152 THP-1 IFIT1-luc cells (Figure 2D, Figure S2E). Vpr expression appeared to mediate a

153 generalized suppression of innate immune activation because it also reduced the activation of
154 IFIT1-luc by Sendai Virus infection, which is mediated by MDA5 and RIGI RNA sensing
155 (Andrejeva et al., 2004; Rehwinkel et al., 2010) (Figure 2E, Figure S2G). Activation of IFIT1-luc
156 by the TLR4 ligand LPS was also reduced by Vpr expression in a dose-dependent manner
157 (Figure 2F, S2H).
158
159 **Vpr inhibition of innate immune activation is dependent on DCAF1 but independent of cell**
160 **cycle arrest**
161 In order to separate innate immune antagonism by Vpr from other Vpr functions, we identified an
162 inactive Vpr mutant. HIV-1 SUMA Vpr F34I/P35N was effectively incorporated into p8.91 derived
163 HIV-1 particles when expressed *in trans* in transfected 293T cells (Figure 3A). HIV-1 GFP
164 particles bearing wild type Vpr, but not Vpr F34I/P35N, effectively suppressed IFIT1-luc
165 expression in THP-1 induced by 5μg/ml cGAMP, added at the time of infection, by an order of
166 magnitude (Figure 3B). Vpr degrades specific target proteins, e.g. the cellular protein UNG2, by
167 recruiting the Cul4 E3 Ubiquitin ligase complex via the substrate recognition component DCAF1
168 (Ahn et al., 2010). The Vpr mutant Q65R fails to recruit DCAF1, and therefore cannot degrade
169 target proteins (Laguette et al., 2014). Vpr Q65R also efficiently incorporated into HIV-1 GFP
170 particles (Figure 3A), but barely suppressed IFIT1-luc induction by cGAMP in THP-1 cells (Figure
171 3B), when delivered by viral particles. Concordantly, shRNA mediated depletion of DCAF1 in
172 THP-1 also prevented Vpr from inhibiting cGAMP induction of IFIT1-luc (Figure 3C). Neither
173 DCAF1 depletion, nor cGAMP treatment reduced infectivity of HIV-1 GFP vector (Figure S3A).
174 Vpr was active in cells expressing a non-targeting shRNA (shControl) and suppressed IFIT1-luc
175 induction. Expression of empty (no Vpr) vector had no effect on IFIT1-luc induction (Figure 3C).
176 Effective depletion of DCAF1 was evidenced by immunoblot (Figure 3D).
177
178 Importantly, Vpr has been shown to arrest cell cycle via SLX4 complex modulation (Laguette et
179 al., 2014; Zhang & Bieniasz, 2019) Indeed, Vpr expression in THP-1 cells induced a significant
180 increase of cells in G2/M phase of cell cycle, measured by labeling DNA with propidium iodide,
181 visualized by flow cytometry (Figure 3E). Expression of Vpr F34I/P35N, which cannot effectively
182 suppress cGAMP mediated IFIT1-luc/ISG expression (Figure 3B, 3G), also induced G1/M cell
183 cycle arrest, albeit slightly less efficiently than wild type Vpr protein (Figure 3E). Conversely, Vpr
184 R80A, previously shown to be defective in inducing cell cycle arrest (Laguette et al., 2014), did
185 not increase the number of cells in G2/M (Figure 3E). Data in Figure 3E are quantified in Figure
186 S3G. Importantly, VprR80A was packaged into HIV-1 particles (Figure 3A), and suppressed
187 IFIT1-luc activation by cGAMP in THP-1 (Figure 3B). These data genetically separate the effect
188 of Vpr expression on cell cycle, and inhibition of innate immune activation, suggesting that these
189 Vpr activities depend on manipulation of different target proteins. It is striking that amino acids at
190 positions 34/35 and 80 are close in Vpr structures and distant from the UNG2 binding site,

191 suggesting an additional target binding interface, as seen in the highly related Vpx protein
192 (Figure S3B, C) (Morellet et al., 2003; Schwefel et al., 2014; Wu et al., 2016). The DCAF1 Vpr
193 binding mutant Q65R did not inhibit cell cycle, as reported (Figure 3E) (Laguette et al., 2014).
194 Expressed Vpr had similar mutation sensitivity as Vpr delivered by HIV-1 particles (compare
195 Figures 3F and 3B). Expression of wild type Vpr and Vpr R80A prevented cGAMP activation of
196 the IFIT1-luc reporter (Figure 3F) and of endogenous *MxA* in THP-1 cells (Figure 3G, S3D). HT
197 DNA transfection, but not lipofectamine alone, activated IFIT1-luc reporter expression, as
198 expected, and this was also sensitive to wild type and VprR80A expression but not expression of
199 Vpr F34I/P35N (Figure S3E, S3F). Vpr Q65R had only a small inhibitory effect in this assay.
200
201 **Wild Type Vpr, but not sensing antagonism inactive Vpr mutants, colocalize with nuclear**
202 **pores**
203 Having identified Vpr mutants defective for antagonism of innate immune sensing, we sought
204 further clues for Vpr mechanism by examining wild type and mutant Vpr location within cells. Vpr
205 expressed in isolation is found in the nucleus and associated with nuclear pores (Fouchier et al.,
206 1998; Le Rouzic et al., 2002). Concordantly, we found FLAG-Vpr (green) in the nucleus and
207 colocalized with antibody staining the nuclear pore complex when expressed by transient
208 transfection in HeLa cells (Figure 4A, B). Strikingly, the Vpr mutants F34I/P35N and Vpr Q65R,
209 which did not suppress PAMP activation of IFIT1-luc/ISG expression (Figure 3) were
210 mislocalized, as compared to wild type and R80A Vpr, which are both active against the
211 consequences of PAMP sensing (Figure 3). Vpr mutants F34I/P35N and Q65R appeared
212 qualitatively different inside the nucleus, and nuclear rim staining was less well defined,
213 suggesting that they have lost interactions with a protein(s) that normally influences their position
214 within the cell. Association between Vpr (green) and the nuclear rim, stained with anti-nuclear
215 pore complex antibody mAb414 (red), was assessed by comparing the fluorescence intensity of
216 the red (NPC) and green (Vpr) signal across the nucleus along the white line (Figure 4C). In
217 single confocal images, fluorescence intensity of the nuclear rim stain showed two distinct peaks
218 representing each edge of the nucleus, and these overlapped with WT and Vpr R80A
219 fluorescence but not with Vpr F34I/P35N or Vpr Q65R fluorescence, which was more diffuse and
220 less well defined at the nuclear rim. Cellular DNA was counter stained with DAPI (blue).
221
222 Vpr has been described to interact with cyclophilin A (CypA) and mutating Vpr residue P35 was
223 reported to prevent this interaction (Zander et al., 2003). The nuclear pore complex has
224 cyclophilin-like domains, which are structurally very similar to CypA, at the end of the Nup358
225 fibers that protrude into the cytoplasm (Schaller et al., 2011). To test whether Nup358 was
226 required for Vpr association with the nuclear rim, we expressed FLAG-Vpr in Nup358-depleted
227 HeLa cells (Schaller et al., 2011) and stained the Vpr FLAG tag (green) and NPC (red) (Figure
228 S4A, B). Despite effective Nup358 depletion (Figure S4C), Vpr remained associated with the

229 nuclear rim (Figure S4A, B, D). This suggested that Nup358 is not required for Vpr nuclear rim
230 association.
231
232 **Vpr inhibits IRF3 nuclear translocation**
233 Given that Vpr is associated with the nuclear rim, and Vpr mutants that break antagonism of
234 innate sensing are mislocalized, we hypothesized that Vpr may act at nuclear pores to influence
235 nuclear transport of inflammatory transcription factors. This would be consistent with previous
236 reports of Vpr influencing nuclear transport, for example, of viral nucleic acids (references PMID
237 27181198, 8041786, 9463369) and inhibiting sensing of HIV-1 26656698. cGAMP is produced
238 by activated cGAS and is recruited by STING, which then forms an active kinase complex in
239 which TBK1 phosphorylates STING, TBK1 itself and the transcription factor IRF3 (Liu et al.,
240 2015; Zhang et al., 2019). IRF3 phosphorylation promotes nuclear translocation and subsequent
241 activation of gene expression including type 1 IFNs (Chen et al., 2008). As expected, transfection
242 of THP-1 cells with HT DNA induced phosphorylation of STING, TBK1 and IRF3-S386,
243 measured by immunoblot, compare lanes 1-3 with lanes 4-6 (Figure 5A). Measurement of IFIT1-
244 luc expression in the same samples, which were split and extracted for immunoblot, indicated
245 effective induction of IFIT1-luc by HT DNA transfection and its inhibition by Vpr expression, but
246 not empty vector (Figure 5B). Strikingly, Vpr expression did not impact STING, TBK1 or IRF3
247 protein levels, or their phosphorylation status, measuring IRF3 phosphorylation at S386,
248 compare lanes 4 and 5 with lane 6 (Figure 5A). Infection levels of Vpr encoding, and empty
249 vector, were similar (Figure S5A). Empty vector expression also had no detectable effect on
250 protein levels or phosphorylation (Figure 5A). Actin was detected as a loading control and Vpr
251 was expressed at a vector MOI of about 1 (Figure S5A). A second example of this experiment is
252 presented in (Figure S5B-E). IRF3 is phosphorylated at multiple sites during activation including
253 at IRF3 S-396. We therefore examined IRF3 S-396 phosphorylation using a phospho-IRF3-S396
254 specific antibody and flow cytometry because this antibody didn't work well by immunoblot. We
255 found that in this case, Vpr delivery by VLP did reduce phosphorylation of IRF3-S-396 after
256 stimulation by either cGAMP or HT DNA in THP-1 cells (Figure 5C). In these experiments, Vpr
257 was delivered by genome free virus like particles made by transfection of 293T cells with p8.91,
258 VSV-G and pcDNA3.1 expressing Vpr *in trans*, as before (Figure 1).
259
260 Given that STING, TBK1 and activating IRF3-S386 phosphorylation status were not inhibited by
261 Vpr expression, we investigated the effect of Vpr on IRF3 nuclear translocation after cGAMP
262 treatment of THP-1. In these experiments, THP-1 were differentiated with 50ng/ml phorbol-12
263 myristate acetate (PMA) to attach them to glass for microscopy. Vpr expression, using titration of
264 Vpr encoding pCSVIG, reduced cGAMP-stimulated IRF3 nuclear translocation, illustrated by
265 immunofluorescent labeling of IRF3 (Figure 5D, E, S5F). Nuclear translocation was quantified by
266 dividing nuclear by cytoplasmic staining intensities for individual cells, measured on a Hermes

267 WISCAN microscope, and plotting translocation coefficients in dot plots (Rasaiyaah et al., 2013)
268 (Figure 5D, E). As a negative control, infection of THP-1 with empty vector had no effect on IRF3
269 translocation (Figure 5D, E). Data in Figure 5D are plotted as a bar chart counting IRF3 positive
270 nuclei, assessed by defining a threshold that clearly splits IRF3 positive and negative nuclei
271 populations in the dot plot (Figure 5D, E). Importantly, suppression of IRF3 nuclear translocation
272 by Vpr was sensitive to Vpr mutation, with the same specificity as before (Compare Figure 3, 4,
273 5F, S5G-J). Vpr F34I/P35N and Vpr Q65R failed to efficiently suppress IRF3 nuclear localization
274 after cGAMP stimulation (Figure 5F, S5G) or after transfection of differentiated THP-1 with HT
275 DNA (Figure 5G, S5H). Conversely, wild type Vpr and Vpr R80A effectively suppressed IRF3
276 nuclear localization after stimulation with cGAMP or HT DNA (Figure 5F, G S5G, H). Similar
277 inhibition specificity by Vpr was also seen after activation of IRF3 nuclear translocation by
278 transfection with the RNA mimic poly I:C (Figure S5I, J).
279
280 **Vpr inhibits NF-κB p65 nuclear translocation and NF-κB sensitive plasmid expression**
281 DNA sensing by cGAS is known to activate NF-κB as well as IRF3 (Fang et al., 2017). To test
282 whether Vpr influenced NF-κB activation we repeated the experiment in Figure 1C-F but using
283 THP-1 cells bearing an NF-κB -luciferase reporter (NF-κB-luc) (Figure 6A-C). VSV-G
284 pseudotyped HIV-1 GFP vector bearing Vpr (packaging construct p8.2) did not particularly
285 activate NF-κB-luc expression, whereas high dose HIV-1 GFP made without Vpr (packaging
286 construct p8.91), activated NF-κB-luc expression effectively (Figure 6A). Activation was
287 dependent on viral genome because similar doses of HIV-1 VLP, made without genome plasmid,
288 did not induce NF-κB-luc expression (Figure 6A). Viral doses were equalized by measurement of
289 RT activity (SGPERT) (Vermeire et al., 2012). Vpr positive, and Vpr negative, HIV-1 GFP were
290 equally infectious and genome-free VLP were not infectious, as expected (Figure 6B). Vpr
291 expression in THP-1 using pCSVIG vector, but not empty vector expression, suppressed
292 subsequent cGAMP-mediated activation of the NF-κB-sensitive gene *IL6* (Figure 6C). We could
293 not detect NF-κB nuclear localization in THP-1 after cGAMP treatment of THP-1, perhaps due to
294 timing, so we tested mutant Vpr specificity using poly I:C to stimulate NF-κB nuclear localization
295 in differentiated THP-1. We found that Vpr inhibited NF-κB nuclear localisation with similar
296 sensitivity to mutation as for IRF3. Activation of NF-κB nuclear translocation by poly I:C,
297 measured by immunofluorescence in the same way as IRF3 nuclear localization, was
298 suppressed by wild type Vpr and Vpr R80A but not by Vpr F34I/P35N or Vpr Q65R (Figure 6D,
299 S6B).
300
301 Previous work has shown that Vpr inhibits the activity of the human CMV immediate early
302 (CMVie) promoter (X. Liu et al., 2015). We hypothesized that this effect may be due to the
303 dependence of this promoter on NF-κB (DeMeritt et al., 2004). As expected Flag-Vpr expression
304 suppressed GFP expression from a co-transfected CMVie – GFP construct (Figure 6E) as well

305 as several other NF-κB sensitive constructs expressing luciferase (Figure S6A). Importantly, Vpr
306 mutants F34I/P35N and Vpr Q65R suppressed GFP expression much less effectively that WT
307 Vpr or Vpr R80A, concordant with this being due to inhibition of transcription factor nuclear entry
308 (Figure 6E, S6D, E). To probe this further, we expressed GFP from two constructs not expected
309 to be NF-κB sensitive because they do not bear any obvious NF-κB binding sites. We used a
310 construct in which GFP is driven from the Ubiquitin C (Ub) promoter (Matsuda & Cepko, 2004) or
311 from the elongation factor 1 alpha (EF1α) promoter (Matsuda & Cepko, 2004). Expression of
312 GFP from the Ub and EF1α promoter were only very slightly reduced by Vpr co-expression but
313 GFP expression from the CMVie promoter was reduced as before (Figure 6F). This correlated
314 with promoter sensitivity to NF-κB because CMVie-GFP expression was induced by activation of
315 NF-κB with exogenous tumour necrosis factor alpha (TNFα) whereas Ub-GFP and EF1α-GFP
316 were not (Figure 6G, S6E-F). Thus, the suppression of activated NF-κB nuclear transport likely
317 explains the observation that Vpr suppresses expression from a CMVie promoter but not
318 promoters that are independent of NF-κB activity for expression.
319
320 **HIV-1 Vpr interacts with karyopherins and inhibits NF-κB (p65) and IRF3 recruitment**
321 WT Vpr suppresses nuclear entry of IRF3 and NF-κB, but Vpr DCAF1 binding mutant Q65R
322 does not (Figure 5, 6). This suggested that Vpr might degrade particular nuclear transport
323 proteins to exert its effect. We therefore tested whether Vpr expression caused degradation of
324 karyopherins KPNA1, KPNA2, KPNA3, KPNA4, KPNA5, KPNA6 or KPNB1. We infected cells
325 with Vpr bearing HIV-1, extracted total protein 48 hours after infection, and detected each protein
326 using immunoblot and specific antibodies (Figure 7A). However, we did not detect reduced levels
327 of any of these karyopherins. It is possible that Vpr recruits karyopherins but does not degrade
328 them. To test this, we sought interaction between Vpr and karyopherins KPNA1, KPNA2 and
329 KPNA3 by co-immunoprecipitation. We found that immunoprecipitation of wild type HA-Vpr co-
330 precipitated Flag-KPNA1 and to a lesser degree Flag-KPNA2 and Flag-KPNA3, but not Flag-
331 tagged GFP (Figure 7B). In a second experiment we tested whether KPNA1-3 interacted with the
332 inactive Vpr mutant F34I/P35N. In this experiment WT Vpr interacted with KPNA1 as before, with
333 less efficient interaction with KPNA2 and KPNA3 (Figure 7C). Importantly, in this experiment
334 KPNA1 interacted with the Vpr F34I/P35N only very weakly, and much less than WT Vpr,
335 consistent with the mutant's reduced activity in antagonizing innate immune sensing (Figure 7C).
336 Given that Vpr expression did not cause KPNA1 degradation, we sought evidence for Vpr
337 disturbing interactions between KPNA1 and IRF3 or NF-κB p65. HA-IRF3 immunoprecipitated
338 with Flag-KPNA1 as expected and this interaction was reduced by expression of WT Vpr, but not
339 inactive mutant Vpr F34I/P35N (Figure 7D). A similar competing immunoprecipitation experiment
340 with KPNA1 and NF-κB p65 gave similar results. Immunoprecipitation of Flag-KPNA1 co-
341 precipitated NF-κB p65 and this was reduced by co-expression of WT Vpr, but not Vpr
342 F34I/P35N (Figure 7E). We conclude that Vpr interacts with KPNA1, and possibly other KPNA

343 proteins, and prevents them from efficiently recruiting and transporting transcription factors IRF3
344 and NF-κB into the nucleus after innate immune activation.
345
346 **Discussion**
347 Here we have provided evidence that Vpr interacts with karyopherin KPNA1 (Figure 7) to inhibit
348 nuclear transport of IRF3 and NF-κB (Figure 5, 6) and subsequent gene expression changes
349 downstream of innate immune sensing (Figures 1-3). Thus, Vpr antagonizes the consequences
350 of innate immune activation by DNA sensing, explaining its ability to rescue HIV-1 replication in
351 cGAMP-treated macrophages (Figure 1). We propose that Vpr provides an *in vivo* replication
352 advantage because activation of IRF3 and NF-κB induces expression of inflammatory cytokines,
353 including type 1 IFNs, and subsequently restriction factors for which HIV-1 does not encode
354 antagonists. For example, IFN induces MxB (Goujon et al., 2013; Kane et al., 2013), IFITM1-3 (T
355 L Foster et al., 2016) and TRIM5α (Jimenez-Guardeño et al., 2019) all of which inhibit HIV-1.
356 Concordantly, accidental infection of a lab worker with a Vpr-defective HIV-1 isolate resulted in
357 delayed seroconversion, suppressed viremia and normal T-cell counts without need for anti-viral
358 treatment (Ali et al., 2018).
359
360 Vpr inhibited induction of ISG mRNA and protein expression downstream of various innate
361 immune stimuli suggesting that Vpr is active against a variety of agonists (Figure 2). Broad Vpr
362 activity is explained by our observation that Vpr acts at the level of IRF3 and NF-κB nuclear
363 transport. Vpr localised to the nuclear rim of cells when expressed (Figure 4), also consistent
364 with activity at the level of nuclear transport. We were surprised that Vpr reduced IRF3
365 phosphorylation at S396 but not at S386 (Figure 5). Previous studies have suggested that
366 phosphorylation of IRF3 at S386 is necessary and sufficient for IRF3 activation (Lin et al., 1999;
367 Mori et al., 2004; Schirrmacher, 2015; Servant et al., 2003; Suhara et al., 2000; Yoneyama et al.,
368 1998). Thus our data are consistent with Vpr inhibiting transport of activated IRF3, and
369 phosphorylation at S396 being after phosphorylation at S386, and perhaps occurring in a
370 karyopherin or NPC interaction dependent way. Phosphorylation of IRF3 at S396 has been
371 associated with enhanced association and multimerization with transcriptional coactivator CREB
372 binding protein (CBP/p300) suggesting a later role than phosphorylation at S386 (Chen et al.,
373 2008). It is also possible that the lack of S396 IRF3 phosphorylation is a consequence of Vpr-
374 mediated suppression of IRF3 nuclear import i.e. dephosphorylation at S396 if nuclear entry is
375 prevented.
376
377 It is noteworthy that the Vpr DCAF1 binding mutant Vpr Q65R was somewhat mislocalised
378 suggesting a role for DCAF1 in defining Vpr location in addition to facilitating target protein
379 degradation (Figure 4). Previous work has also associated DCAF1 with Vpr localisation (Zhang
380 et al., 2001). Vpr F34I/P35N (Figure 4) was also mislocalised, consistent with its failure to

381 interact efficiently with KPNA1 (Figure 7). Importantly, both Vpr mutants Q65R and F34I/P35N,
382 were non-functional in antagonism of innate stimuli measured by ISG expression (Figure 3),
383 IRF3/NF-κB nuclear translocation (Figure 5, 6) and inhibition of plasmid expression (Figure 6).
384 Thus Vpr location and activity are likely governed by interaction with both DCAF1 and KPNA
385 proteins.
386
387 Classical nuclear import of proteins is carried out via karyopherins, or importins, recruitment of a
388 canonical basic NLS in protein cargoes. The transporter complexes solubilise cargoes in the
389 Phe-Gly (FG) matrix that fills the central nuclear pore complex channel formed by FG repeats
390 contributed by NPC associated proteins. The regulation of the nuclear import of NF-κB and IRF3
391 by multiple karyopherins is expected to be complex (Fagerlund et al., 2005, 2008; Kumar et al.,
392 2002; Liang et al., 2013). Targeting karyopherins is a typical viral strategy for manipulation of
393 cellular responses and the different ways viruses perform this function hints at the complexity
394 involved. For example, Japanese encephalitis virus NS5 targets KPNA2, 3 and 4 to prevent IRF3
395 and NF-κB nuclear translocation (Ye et al., 2017). Hantaan virus nucleocapsid protein inhibits
396 NF-κB p65 translocation by targeting KPNA1, -2, and -4 (Taylor et al., 2009). Most recently,
397 vaccinia virus protein A55 was shown to interact with KPNA2 to disturb its interaction with NF-κB
398 (Pallett et al., 2019). Hepatitis C virus NS3/4A protein restricts IRF3 and NF-κB translocation by
399 cleaving KPNB1 (importin-β) (Gagne et al., 2017). We propose that the different mechanisms of
400 NF-κB/IRF3 manipulation by viruses reflect their reliance on transcriptional activation while
401 simultaneously depending on inhibition of transcription factors taking part in defensive
402 processes. We hypothesise that each virus has specifically adapted to manipulate nuclear
403 transport of transcription factors to facilitate replication while dampening inflammatory responses
404 downstream of pattern recognition receptors. This is consistent with Vpr inhibiting NF-κB p65
405 despite depending on NF-κB activity for enhancement of viral transcription (Griffin et al., 1989).
406 One possibility is that once Gag is expressed, Gag recruits Vpr to viral particles to prevent further
407 manipulation of nuclear transport (Belzile et al., 2010).
408
409 Vpr has previously been shown to interact with KPNA1, 2 and 4 (Nitahara-Kasahara et al., 2007;
410 Takeda et al., 2011; Vodicka et al., 1998). Here we confirm an interaction with KPNA1 by co-
411 immunoprecipitation that is reduced by Vpr mutation F34I/P35N, which does not impact cell cycle
412 manipulation, but prevents antagonism of innate immune sensing. Importantly we did not
413 observe degradation of any karyopherins tested in the presence of Vpr, rather Vpr prevented
414 interaction of KPNA1 with IRF3 and NF-κB p65. This suggests that some KPNA1 nuclear import
415 function may be left intact by the virus to facilitate a more subtle manipulation of host cell biology
416 (Figure 7). A similar model of inhibition of KPNA target binding to manipulate nuclear import has
417 been suggested by a crystal structure of Ebola Virus VP24 protein in complex with KPNA5. This

418 study proposed that VP24 targets a KPNA5 NLS binding site to specifically inhibit nuclear import
419 of phosphorylated STAT1 (W. Xu et al., 2014).
420
421 Our data also likely explain previous reports of the suppression of expression from co-
422 transfected CMV promoter-driven plasmids by Vpr (X. Liu et al., 2015). The fact that NF-κB-
423 independent and TNFα-insensitive ubiquitin and EF1α promoters were not sensitive to Vpr is
424 consistent with this model (Figure 6). It is likely that inhibition of NF-κB nuclear transport inhibits
425 expression from the NF-κB-dependent CMV promoter, but another possibility is that transcription
426 factor bound to cytoplasmic plasmid DNA has a role in importing DNA into the nucleus, and it is
427 plasmid transport that is inhibited (Mesika et al., 2001). Our model is summarized in Figure S7.
428
429 Importantly, our data suggest that manipulation of cell cycle by Vpr is independent of
430 manipulation of IRF3 and NF-κB nuclear transport. The Vpr R80A mutant, which does not arrest
431 cell cycle, or manipulate SLX4 complex (Gaynor & Chen, 2001; Laguette et al., 2014) was
432 functional in inhibition of innate sensing (Figures 3, 5, 6). Mapping the residues of Vpr that are
433 important for innate immune inhibition onto structures resolved by NMR and X-ray
434 crystallography reveals a potentially distinct interface from that targeting UNG2 (Figure S3).
435 Residues Vpr 34/35 are distant from the UNG2 binding site but R80 is close in the 3D structure.
436 Given that Vpr has been shown to bind FxFG motif in p6 of Gag during virion incorporation (Zhu
437 et al., 2004), and FG motifs at the NPC (Fouchier et al., 1998) it is possible that Vpr also
438 manipulates transport across the nuclear pore through FG motif recruitment at the NPC.
439
440 Virus transmission is essential for their survival and so selective pressures applied by defensive
441 host innate immunity at the time of transmission is expected to be important. We hypothesise a
442 critical role for Vpr in viral transmission. Association between activation of innate sensing and
443 transmission is suggested by evidence of low HIV transmission frequency (Shaw & Hunter,
444 2012), HIV founder clones being particularly resistant to IFN (Iyer et al., 2017) as well activation
445 of a dramatic cytokine cascade at the time of transmission (Stacey et al., 2009). Concordantly,
446 Vpu, Nef and Vif, and now Vpr, antagonize innate immunity to enhance viral replication, reviewed
447 in Sumner et al., 2019. Given that HIV-1 is very sensitive to type 1 IFN, we imagine that the IFN
448 recorded in peripheral blood at the time of transmission (Stacey et al., 2009), occurs either after
449 transmission is established, or occurs in compartments that are separated, or distant from, the
450 effectively transmitted virus.
451
452 We and others, have argued that the genome of wild type HIV-1 is not efficiently sensed by
453 nucleic acid sensors, or degraded by cellular nucleases, because the capsid protects HIV-1
454 genome, and regulates the process of reverse transcription, during transport across a hostile
455 cytoplasmic environment, prior to uncoating at the NPC, or in the nucleus of infected cells

456 (Bejarano et al., 2019; Burdick et al., 2017; Francis et al., 2016; Jacques et al., 2016; Rasaiyaah
457 et al., 2013; Schaller et al., 2011; Yan et al., 2010; Zila et al., 2019) (Rebecca P Sumner et al.,
458 2019). However, other studies have demonstrated sensing of wild type HIV-1 DNA by cGAS
459 (Gao et al., 2013; Lahaye et al., 2013; Yan et al., 2010), and here we observed cGAS-
460 dependent, Vpr-sensitive, induction of CXCL10 by high dose VSV-G pseudotyped single round
461 HIV-1 GFP vector in THP-1 cells. We propose that both capsid and Vpr have a role in preventing
462 HIV-1 stimulating innate immune sensing and that both are required for the lowest levels of
463 activation, particularly to promote replication *in vivo* (Ali et al., 2018). *In vitro*, primary myeloid
464 cells behave according to the stimuli they have received. Thus, inconsistent results between
465 studies could be explained by differences in myeloid cell stimulation due to differences in cell
466 purification and differentiation methods or reagents used. Methods of virus purification, here
467 performed by centrifugation through sucrose, may also be a source of target cell activation and
468 experimental variation. Here, we observed cGAMP induction of Vpr dependence in MDM (Figure
469 1). Replication in activated primary CD4+ T cells was, in our hands, independent of Vpr in the
470 presence and absence of cGAMP, which was inhibitory, suggesting that Vpr cannot overcome
471 signalling downstream of cGAMP in these cells. This implies that activated T-cells respond
472 differently to cGAMP than macrophages, consistent with a previous study suggesting that in
473 Tcell/macrophage mixed cultures, the negative effects of cGAMP on HIV-1 replication was
474 principally mediated via macrophages (Xu et al., 2016).
475
476 In summary these findings highlight the crucial role of particle associated Vpr in inhibiting innate
477 immune activation during the early stages of the viral life cycle. We propose that the further study
478 of viral inhibition of inflammatory signalling downstream of pathogen sensing may lead to a better
479 understanding of the complexity of PAMP-driven inflammatory responses and highlight tractable
480 novel targets for therapeutic anti-inflammatory development.
481
482 **Acknowledgements**
483 We thank Veit Hornung for providing THP-1-IFIT-1 cells wild type and knock outs, Geoffrey
484 Smith for providing constructs encoding KPNA1-3 and Clare Jolly and Richard Sloan for
485 providing NL4.3ΔVpr. This work was funded through an MRC PhD studentship (HK) an MRC
486 Clinical Training Fellowship (CVT), a Wellcome Trust clinical training fellowship (DF), a
487 Wellcome Trust Senior Biomedical Research Fellowship (GJT), the European Research Council
488 under the European Union's Seventh Framework Programme (FP7/2007-2013)/ERC (grant
489 HIVInnate 339223) (GJT), a Wellcome Trust Collaborative award (GJT) and was supported by
490 the National Institute for Health Research University College London Hospitals Biomedical
491 Research Centre.
492
493 **Author contributions**

494 HK, RPS, LZA, LT, DF and GJT conceived the study. HK, RPS, JR, CPT, MTRP, CVT and DS
495 performed experiments. HK, RPS and GJT analyzed the data. HK, RPS and GJT wrote the
496 manuscript.
497
498 **Star Methods**
499
500 **Cells and reagents**
501 HEK293T cells were maintained in DMEM (Gibco) supplemented with 10 % foetal calf serum
502 (FCS, Labtech) and 100 U/ml penicillin and 100 µg/ml streptomycin (Pen/Strep; Gibco). THP-1
503 cells were maintained in RPMI (Gibco) supplemented with 10% FCS and Pen/Strep. THP-1-IFIT-
504 1 luciferase reporter cells express Gaussia luciferase under the control of the endogenous IFIT1
505 promoter have been described (Mankan et al., 2014). THP-1 CRISPR control, *cGAS-/-* and
506 *MAVS -/-* knockout cells have been described (Mankan et al., 2014). Nup358 depleted HeLa
507 cells have been described (Schaller et al., 2011). Lipopolysaccharide, poly I:C and TNFα were
508 obtained from PeproTech. Sendai virus was obtained from Charles River Laboratories. Herring-
509 testis DNA was obtained from Sigma. cGAMP was obtained from Invivogen. NF-κB Lucia THP-1
510 reporter cells were obtained from Invivogen.
511
512 **Cloning and plasmids**
513 The Vpr gene from HIV-1 founder clone SUMA (Fischer et al., 2010) was codon optimised and
514 synthesised by GeneArt. To generate the HIV-1 vector encoding Vpr (pCSVIG), the codon
515 optimised SUMA Vpr gene was cloned into pSIN-BX-IRES-Em between BamHI and XhoI sites
516 under the control of the SFFV LTR promoter. pSIN-BX-IRES-Em was obtained from Dr Yasuhiro
517 Takeuchi. EF1α-GFP and UB-GFP were obtained from Addgene (Matsuda & Cepko, 2004). The
518 CMV-GFP construct was pEGFPC1 (Clontech). HIV-1 bearing a Ba-L envelope gene has been
519 described (Rasaiyaah et al., 2013). Flag- KPNA1-3 plasmids were obtained from Prof. Geoffrey
520 Smith. HIV-1ΔVpr was a gift from Richard Sloan and encoded an 17 nucleotide insertion (Vpr 64-
521 81) that destroys the Vpr coding sequence.
522
523 **Production of virus in HEK293T cells**
524 Replication competent HIV-1 and HIV-1 GFP vectors were produced by transfection of HEK293T
525 cells in T150 flasks using Fugene 6 transfection reagent (Promega) according to the
526 manufacturer's instructions. Briefly, just-subconfluent T150 flasks were transfected with 8.75 µg
527 of HIV-1 YU2 or HIV-1 YU2 lacking Vpr (HIV-1 YU2 ΔVpr) and 30 µl Fugene 6 in 500 µl Optimem
528 (Thermofisher Scientific). To make VSV-G pseudotyped HIV-1 GFP, each T150 flask was
529 transfected with 2.5 µg of vesicular stomatitis virus-G glycoprotein encoding plasmid (pMDG)
530 (Genscript), 2.5 µg of packaging plasmid, p8.91 (encoding Gag-Pol, Tat and Rev) or p8.2
531 (encoding Gag-Pol, Tat and Rev and Vif, Vpr, Vpu and Nef) (Zufferey et al., 1997), and 3.75 µg

532 of GFP encoding genome plasmid (pCSGW) using 30 µl Fugene 6 in 500µl optimum. To make
533 Vpr encoding HIV-1 GFP, 3.75 µg pCSVIG was transfected with 2.5 µg of pMDG and 2.5 µg of
534 p8.91. To make HIV-1 GFP particles bearing Vpr, 1 µg of Vpr expressing pcDNA3.1 (wild type
535 SUMA Vpr or Vpr mutants) was transfected with 2.5 µg of pMDG and 2.5 µg of p8.91 in 30ul
536 Fugene-6 and 500µl Optimem. All virus supernatants were harvested at 48 and 72 h post-
537 transfection, replicate flasks were pooled, and supernatants subjected to ultracentrifugation
538 through a 20% sucrose cushion at 23000 rpm for 2 hours in a 30 ml swingout rotor (Sorvall)
539 (72000G). Viral particles were resuspended in RPMI supplemented with 10% FCS. HIV-GFP
540 produced with p8.91 or p8.2 used in Figure 1 were DNase treated for 2 hours at 37°C (DNaseI,
541 Sigma) prior to ultracentrifugation. Viruses were titrated by infecting THP-1 cells (2x10^{5} cells/ml)
542 with dilutions of sucrose purified virus in the presence of polybrene (8 µg/ml, Sigma) and
543 incubating for 48 h. GFP-positive, infected cells were counted by flow cytometry using a BD
544 Accuri C6 (BDBiosciences). HIV-1 vector encoding shRNA targeting DCAF1 has been described
545 and was prepared as above (Berger et al., 2015).
546
547 **SG-PERT**
548 Viral doses were determined by measuring reverse transcriptase activity of virus preparations by
549 qPCR using a SYBR Green-based product-enhanced PCR assay (SG-PERT) as described
550 (Vermeire et al., 2012).
551
552 **Isolation of primary monocyte-derived macrophages and CD4+ T cells from peripheral**
553 **blood**
554 Primary monocyte-derived macrophages (MDM) were prepared from fresh blood from healthy
555 volunteers. Primary CD4+ T cells were obtained from leukocyte cones from healthy donors. The
556 study was approved by the joint University College London/University College London Hospitals
557 NHS Trust Human Research Ethics Committee. Peripheral blood mononuclear cells (PBMCs)
558 were isolated by density gradient centrifugation using Lymphoprep (Stemcell Technologies). For
559 MDM preparation, PBMCs were washed three times with PBS and plated to select for adherent
560 cells. Non-adherent cells were washed away after 1.5 h and the remaining cells incubated in
561 RPMI (Gibco) supplemented with 10 % heat-inactivated pooled human serum (Sigma) and
562 40 ng/ml macrophage colony stimulating factor (R&D systems). Cells were further washed after 3
563 days and the medium changed to RPMI supplemented with 10% heat-inactivated human serum
564 (Sigma). MDM were then infected 3-4 days later at low multiplicity of infection. Spreading
565 infection was detected by Gag staining and counting Gag positive cells as described (Rasaiyaah
566 et al., 2013). For CD4+ T cells, untouched CD4+ T cells were purified from PBMCs with an
567 indirect magnetic labeling system (MACS, Miltenyi Biotec), according to manufacturer's
568 instructions. Cells were then cultured with 2 µg/ml of plate-bound anti-CD3 and anti-CD28
569 monoclonal antibodies (αCD3αCD28 stimulation) (mAbs) (eBioscience) and 25 U/ml of

570 recombinant human interleukin-2 (IL-2; Roche Applied Science) at a concentration of 1.5-2 x 10^6
571 cells/ml in RPMI supplemented with 10% heat-inactivated Human Serum (HS) (SigmaAldrich).
572 Cells were maintained at 37°C in 5% CO_2 in a humidified incubator for 72 h. CD4+ T cells were
573 then assessed for spreading infection of CXCR4-tropic HIV-1 NL4.3 WT and ΔVPR at low
574 multiplicity of infection (300 mU of HIV-1 RT Activity per 1x10^6 cells). Percentage of HIV-1-
575 infected primary CD4+ T cells was determined by flow cytometry measuring p24Gag antigen
576 employing the monoclonal antibody p24Gag-FITC (HIV-1 p24 (24-4), Santa Cruz Biotechnology).
577
578 **Innate immune sensing assays**
579 THP-1 cells were seeded in 96 well plates (5x10^5 cells/ml). For Vpr expression, cells were
580 infected with an empty or Vpr expressing (pCSVIG) lentiviral vectors for 40 hours. For stimulation
581 of cells with HT-DNA or poly I:C, 0.2 µl of lipofectamine and 25 µl of Optimem were incubated
582 with HT-DNA or poly I:C (amounts stated in figure legends) for 20 minutes and added to cells.
583 Lipopolysaccharide (1 µg/ml), TNFα (200 ng/ml), Sendai virus (200 HA U/ml) or cGAMP (5
584 µg/ml) were added directly to the media. For experiments with virion delivered/associated Vpr,
585 cells were stimulated at the time of infection. Gaussia/Lucia luciferase activities were measured 8
586 hours post cell stimulation by transferring 10 µl supernatant to a white 96 well assay plate,
587 injecting 50 µl per well of coelenterazine substrate (Nanolight Technologies, 2 µg/ml) and
588 analysing luminescence on a FLUOstar OPTIMA luminometer (Promega). Data were normalized
589 to a mock-treated control to generate a fold induction.
590
591 **ELISA**
592 Cell supernatants were harvested for ELISA at 8 h post-stimulation and stored at -80 ^{o}C. CXCL-
593 10 protein was measured using Duoset ELISA reagents (R&D Biosystems) according to the
594 manufacturer's instructions.
595
596 **ISG qPCR**
597 RNA was extracted from THP-1 cells using a total RNA purification kit (Norgen) according to the
598 manufacturer's protocol. Five hundred ng RNA was used to synthesise cDNA using Superscript
599 III reverse transcriptase (Invitrogen), also according to the manufacturer's protocol. cDNA was
600 diluted 1:5 in water and 2 µl was used as a template for real-time PCR using SYBR® Green PCR
601 master mix (Applied Biosystems) and a 7900HT Real-Time PCR machine (Applied Biosystems).
602 Expression of each gene was normalised to an internal control (*GAPDH*) and these values were
603 then normalised to mock-treated control cells to yield a fold induction. The following primers were
604 used:
605 *GAPDH:* Fwd 5'-GGGAAACTGTGGCGTGAT-3', Rev 5'-GGAGGAGTGGGTGTCGCTGTT-3'
606 *CXCL-10:* Fwd 5'-TGGCATTCAAGGAGTACCTC-3', Rev 5'-TTGTAGCAATGATCTCAACACG-3'
607 *IFIT-2:* Fwd 5'-CAGCTGAGAATTGCACTGCAA-3', Rev 5'-CGTAGGCTGCTCTCCAAGGA-3'

608 *MxA:* Fwd 5'-ATCCTGGGATTTTGGGGCTT-3', Rev 5'-CCGCTTGTCGCTGGTGTCG-3'
609 *Viperin:* Fwd 5'-CTGTCCGCTGGAAAGTG-3', Rev 5'-GCTTCTTCTACACCAACATCC-3'
610 *IL-6:* Fwd 5'- AAATTCGGTACATCCTCGACG-3', Rev 5'- GGAAGGTTCAGGTTGTTTTCT-3'
611
612 **Immunofluorescence**
613 For confocal microscopy, HeLa cells ($5x10^4$ cells/ml) were seeded into 24-well plates containing
614 sterile glass coverslips. For nuclear translocation assays, THP-1 cells ($4x10^5$ cells/ml) were
615 adhered in an optical 96-well plate (PerkinElmer) with 50 ng/ml phorbol 12-myristate 13-acetate
616 (PMA, Peprotech) for 48 hours. HeLa or adhered THP-1 cells were then washed twice with ice-
617 cold PBS and fixed in 4% (vol/vol) paraformaldehyde. Autofluorescence was then quenched in
618 150 mM ammonium chloride, the cells permeabilized in 0.1% (vol/vol) Triton X-100 in PBS and
619 blocked for 30 min in 5% (vol/vol) FCS in PBS. Cells were incubated with primary Ab for 1 hour
620 followed by incubation with secondary Ab for 1 hour. Cells were washed with PBS three times
621 between each step. The coverslips were placed on a slide prepared with a 30 µl drop of
622 mounting medium (Vectashield, containing 4',6-diamidino-2-phenylindole (DAPI)) and allowed to
623 set before storing at 4° C. Images were taken on a Leica TCS SPE confocal microscope and
624 analyzed in ImageJ. For IRF3/NF-κB(p65) translocation, images were taken on Hermes WISCAN
625 (IDEA Bio-Medical) and analyzed with Metamorph software (Molecular Devices). Metamorph
626 calculated a translocation coefficient representing the proportion of staining in nuclear versus
627 cytoplasmic compartments. A value of 1 represents "all staining in the nucleus", -1 is "exclusively
628 in cytoplasm" and 0 is "equally distributed".
629
630 Primary antibodies were from the following sources: Mouse-anti-FXFG repeats containing
631 nucleoporins (Mab414) (Abcam), Rabbit-anti-flag (Sigma), Rabbit-anti-IRF3 (Santa Cruz
632 Biotechnology) and Mouse-anti-NF-kB p65 (Santa Cruz Biotechnology). Primary antibodies were
633 detected with Goat-anti-rabbit Alexa Fluor 488 IgG (Invitrogen) or Goat-anti-mouse Alexa Fluor
634 546 IgG (Invitrogen).
635
636 **Immunoblotting**
637 For immunoblotting of viral particles, sucrose purified (as described above) virions ($1×10^{11}$ RT
638 units) were boiled for 10 min in 6X Laemmli buffer (50 mM Tris-HCl (pH 6.8), 2 % (w/v) SDS,
639 10% (v/v) glycerol, 0.1% (w/v) bromophenol blue, 100 mM β-mercaptoethanol) before separating
640 on 12 % polyacrylamide gel. Cells were lysed in lysis buffer containing 50 mM Tris pH 8, 150 mM
641 NaCl, 1 mM EDTA, 10% (v/v) glycerol, 1 % (v/v) Triton X100, 0.05 % (v/v) NP40 supplemented
642 with protease inhibitors (Roche), clarified by centrifugation at 14,000 x *g* for 10 min and boiled in
643 6X Laemmli buffer for 10 min. Proteins were separated by SDS-PAGE on 12% polyacrylamide
644 gels. Proteins were transferred to a Hybond ECL membrane (Amersham biosciences) using a
645 semi-dry transfer system (Biorad). Primary antibodies were from the following sources: Rabbit-

646 anti-VSV-G (Sigma), Rabbit-anti-HIV-1 p24 (NIH AIDS reagent program), Rabbit-anti-STING
647 (Cell signaling), Rabbit-anti-pSTING (Cell signaling), Rabbit-anti-TBK1 (Cell signaling), Rabbit-
648 anti-pTBK1 (Cell signaling), Rabbit-anti-IRF3 (Cell signaling), Rabbit-anti-pIRF3-386 (Sigma),
649 Mouse-anti-actin (Abcam), Rabbit-anti-cGAS (Cell Signaling Technology), Mouse-anti-MAVS
650 (Cell Signaling Technology), Rabbit-anti-DCAF1 (Bethyl), Rabbit-anti-Nup358 (Abcam), Mouse-
651 anti-flag (Sigma), Rabbit-anti-GFP (Abcam), KPNA1-6 (ABclonal), KPNB1 (ABclonal), Rabbit-
652 anti-cypB (Abcam), Mouse-anti-FLAG (Sigma), Rabbit-anti-HA (Sigma) and Rabbit-anti-Vpr
653 (NIH). Primary antibodies were detected with goat-anti-mouse/rabbit IRdye 800CW infrared dye
654 secondary antibodies and membranes imaged using an Odyssey Infrared Imager (LI-COR
655 Biosciences).
656
657 **Cell cycle analysis**
658 WT Vpr or Vpr mutants were expressed in THP-1 cells using pCSVIG at an MOI of 1. Cells were
659 incubated for 48 hours and then washed with PBS and fixed in 1 ml cold 70% ethanol on ice for
660 30 minutes. To ensure efficient fixing and minimise clumping, ethanol was added dropwise while
661 vortexing. Cell were pelleted in a microfuge and ethanol was removed followed by two wash
662 steps with PBS. To remove RNA from the samples, RNase A (100 μg/ml) was added and the
663 cells were stained with propidium iodide (PI) (50 μg/ml) to stain cellular DNA. Cells were
664 incubated for 10 minutes at room temperature and DNA content analysed by flow cytometry on a
665 BD FACSCalibur (BD Biosciences). The data were analysed with FlowJo.
666
667 **Generation of Vpr mutants**
668 Site directed mutagenesis was performed using Pfu Turbo DNA Polymerase (Agilent) according
669 to the manufacturer's instructions with the following primers using either pCDNA3.1 or pCSVIG
670 encoding SUMA Vpr as template.
671 VprF34I+P35N: Fwd 5'-GCCGTGCGGCACATCAACAGACCTTGGCTGCATAGC-3',
672 Rev 5'GCTATGCAGCCAAGGTCTGTTGATGTGCCGCACGGC-3'
673 VprQ65R: Fwd 5'-GCCATCATCAGAATCCTGCGGCAGCTGCTGTTCATC-3',
674 Rev 5'-GATGAACAGCAGCTGCCGCAGGATTCTGATGATGGC-3'
675 VprR80A: Fwd 5'-GGCTGCCGGCACAGCGCCATCGGCATCACCCCT-3',
676 Rev 5'-AGGGGTGATGCCGATGGCGCTGTGCCGGCAGCC-3'
677
678 **Co-immunoprecipitation assays**
679 HEK293T cells were grown in 10 cm dishes and co-transfected with plasmids expressing a
680 FLAG-tagged protein (1 µg KPNA1, KPNA2, KPNA3, GFP or empty vector (EV)) and 1 µg of a
681 plasmid expressing HA-tagged SUMA Vpr wild-type, or Vpr F34I/P35N mutant using 6 µl
682 Fugene-6 (Promega). For KPNA-cargo IPs HEK293T cells were grown in 10 cm dishes and co-
683 transfected with 1 µg of a plasmid expressing FLAG-tagged KPNA1, 1 µg of a plasmid

684 expressing HA-tagged p65 or IRF3 and 1 µg of a plasmid expressing un-tagged Vpr,
685 VprF34I+P35N or empty vector control. After 24 h cells were lysed in lysis buffer (0.5 (v/v) % NP-
686 40 in PBS supplemented with protease inhibitors (Roche) and phosphatase inhibitors (Roche),
687 pre-cleared by centrifugation and incubated with 25 µl of mouse-anti-HA agarose beads
688 (Millipore) or mouse-anti-FLAG M2 agarose affinity gel (Sigma) for 2-4 h. Immunoprecipitates
689 were washed 3 times in 1 ml of lysis buffer and eluted from the beads by boiling in 20 µl of 2X
690 sample buffer containing SDS and β-mercaptoethanol. Proteins were resolved by SDS-
691 polyacrylamide gel electrophoresis (NuPAGE 4-12 % Bis-Tris protein gels, Invitrogen) and
692 detected by immunoblotting.
693
694 **Statistical analyses**
695 Data were analysed by statistical tests as indicated in the figure legends. * represent statistical
696 significance: * ($p<0.05$), ** ($p<0.01$), *** ($p<0.001$), **** ($p<0.0001$).
697
698 **Figures**
699

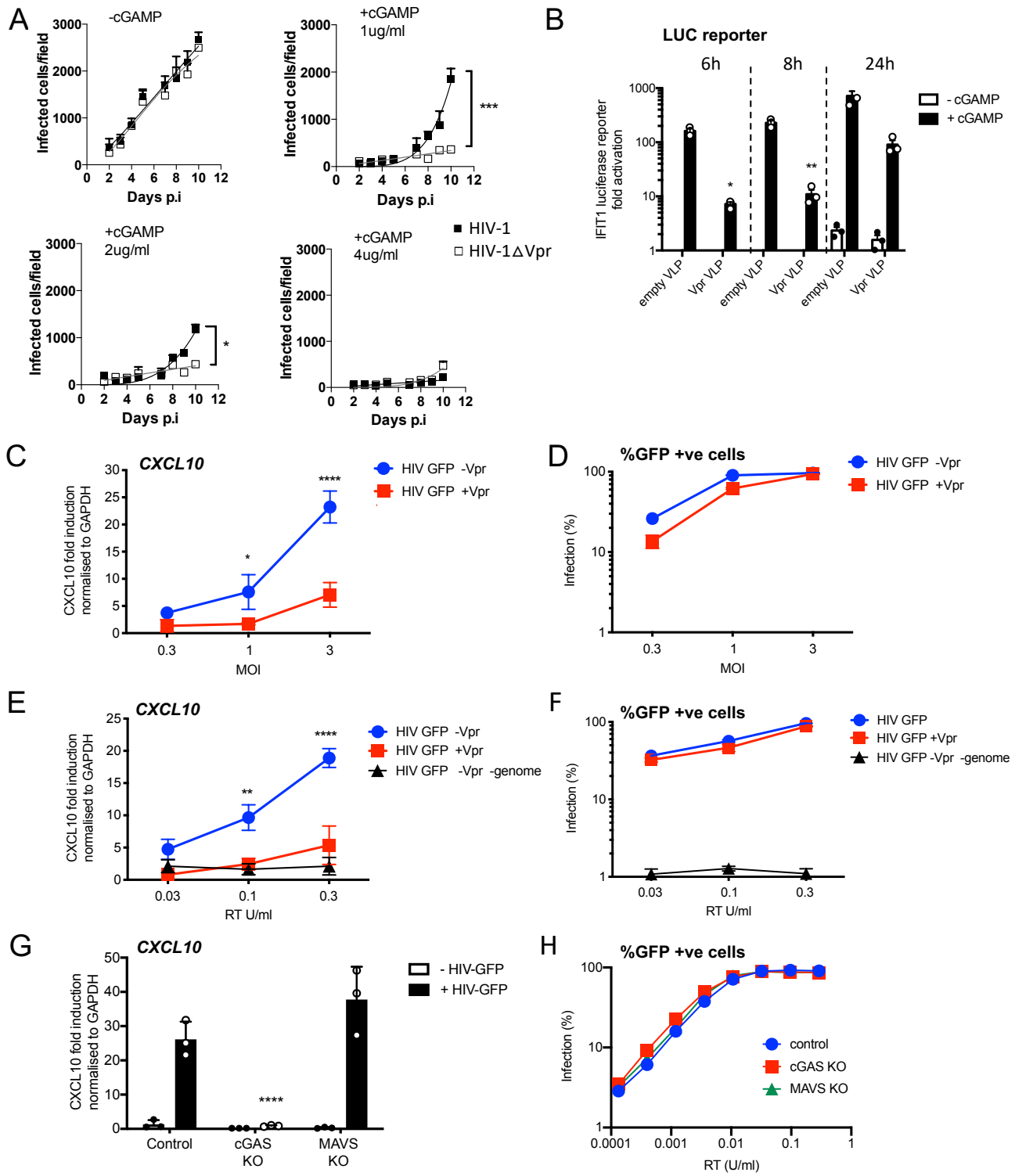

Figure 1 HIV-1 replication in cGAMP stimulated MDMs requires Vpr

(A) Replication of WT Yu2 HIV-1 or Yu2 HIV-1ΔVpr in MDMs stimulated with 1 µg/ml, 2 µg/ml or 4 µg/ml cGAMP or left unstimulated, infection measured by counting Gag positive cells. Mean+/-SEM n=3 1 and 2 µg/ml cGAMP; n=2 4 µg/ml cGAMP. *** = 2 way ANOVA p value <0.001, * = p<0.05.

(B) Fold induction of IFIT1-Luc after activation of STING by cGAMP (5 µg/ml) and infection with WT Vpr-bearing virus like particles (VLP) or empty VLP (1 RT U/ml) in IFIT1-Luc reporter THP1 cells.

711
712 (C) Fold induction of *CXCL10* after infection of THP1 cells with HIV-GFP -Vpr or HIV-GFP +Vpr
713 at the indicated MOI.
714
715 (D) Percentage of THP1 cells infected by HIV-GFP -Vpr or HIV-GFP +Vpr in (C).
716
717 (E) Fold induction of *CXCL10* after infection of THP1 cells with HIV-GFP -Vpr, HIV-GFP +Vpr or
718 HIV-GFP -Vpr lacking genome at indicated doses measured by reverse transcriptase SG-PERT
719 assay.
720
721 (F) Percentage of THP1 cells infected by HIV-GFP -Vpr, HIV-GFP +Vpr or HIV-GFP -Vpr -
722 genome in (E).
723
724 (G) Fold induction of *CXCL10* after infection of control, cGAS-/- or MAVS-/- THP1 knock out cells
725 with HIV-GFP (0.3 RT U/ml).
726
727 (H) Percentage infection of control, cGAS-/- or MAVS-/- THP1 knockout cells infected with HIV-
728 GFP at indicated doses of RT measured by reverse transcriptase SG-PERT assay.
729
730 (B-H) Data are expressed as means ± SD (n = 3) with two-way ANOVA * ($p<0.05$), ** ($p<0.01$),
731 *** ($p<0.001$), **** ($p<0.0001$) compared to empty VLP (B), HIV GFP+Vpr (C, E) and control (G).
732

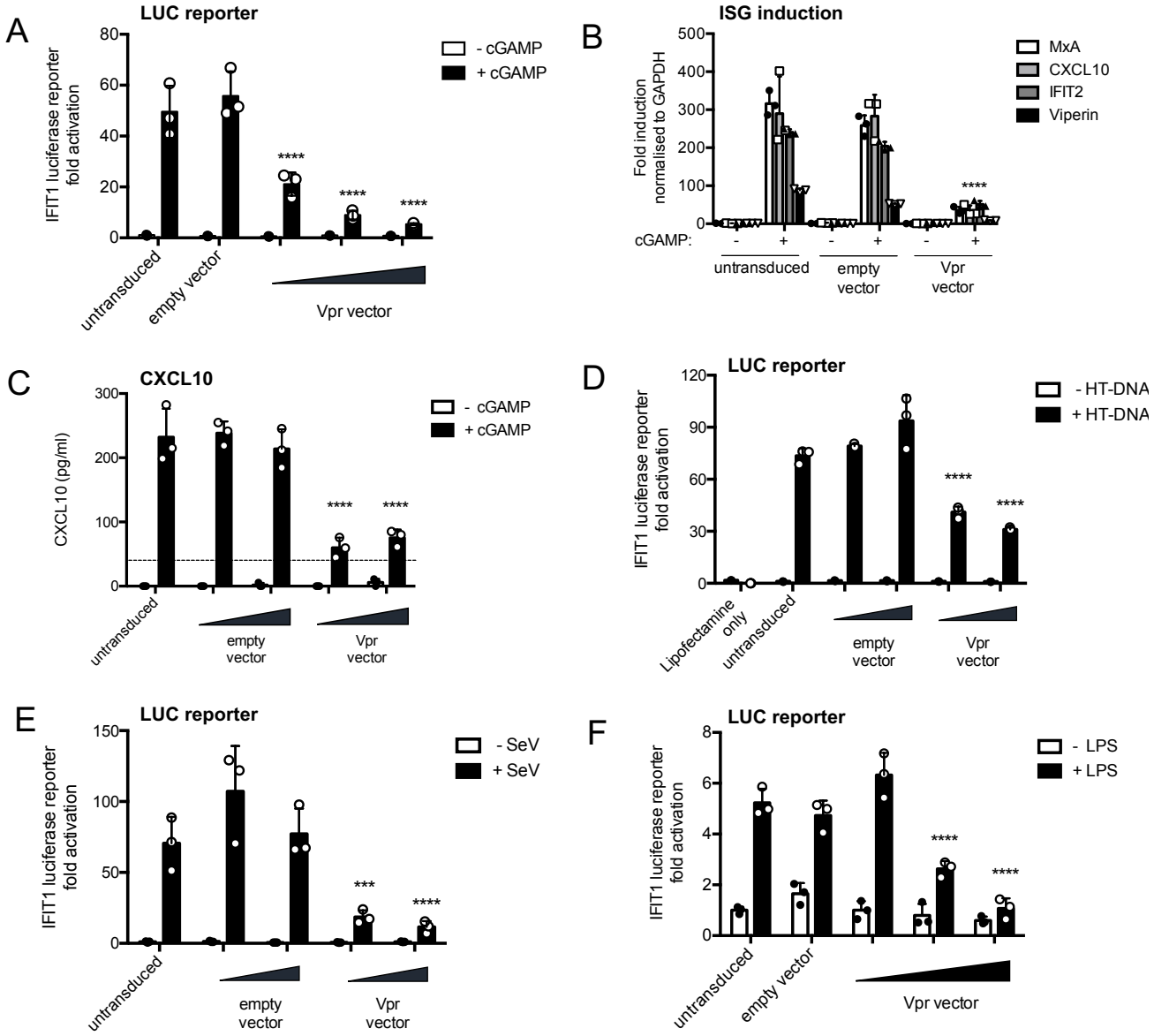

Figure 2 HIV-1 Vpr expression inhibits interferon stimulated gene expression after stimulation with various innate immune stimuli

(A) Fold induction of IFIT1-Luc, after activation of STING by cGAMP (5 µg/ml), in IFIT1-Luc reporter THP1 cells expressing Vpr from a lentiviral vector delivered at MOIs of 0.25, 0.5, 1, or after empty vector transduction (MOI 1) or in untransduced cells.

(B) Fold induction of ISGs *MxA*, *CXCL10*, *IFIT2* and *Viperin* after activation of STING by cGAMP (5 µg/ml) in cells expressing Vpr from a lentiviral vector (MOI 1), or after empty vector transduction (MOI 1) or in untransduced THP1 cells.

(C) Secreted CXCL10 (ELISA) after activation of STING by cGAMP (5 µg/ml) in cells expressing Vpr from a lentiviral vector (MOI 0.5, 1), or after transduction with empty vector (MOI 0.5, 1) or in untransduced THP1 cells. Dotted line shows limit of detection.

(D) Fold induction of IFIT1-Luc after HT-DNA transfection (5 µg/ml) of cells expressing Vpr from a lentiviral vector (MOI 0.5, 1), or empty vector (MOI 0.5, 1) or in untransduced IFIT1-Luc reporter THP1 cells.

754 (E) Fold induction of IFIT1-Luc, after Sendai virus infection, of cells expressing Vpr from a
755 lentiviral vector (MOI 0.5, 1), or after transduction by empty vector (MOI 0.5, 1) or in
756 untransduced IFIT1-Luc reporter THP1 cells.
757
758 (F) Fold induction of IFIT1-Luc, after LPS treatment (1 µg/ml), of cells expressing Vpr from a
759 lentiviral vector (MOI 0.25, 0.5, 1), after transduction by empty vector (MOI 1) or in untransduced
760 IFIT1-Luc reporter THP1 cells.
761
762 Data are expressed as mean ± SD (n = 3) analysed using two-way ANOVA * ($p<0.05$), **
763 ($p<0.01$), *** ($p<0.001$), **** ($p<0.0001$) compared to empty vector. Data are representative of
764 three (A, D-F) or two (B-C) independent experiments.
765

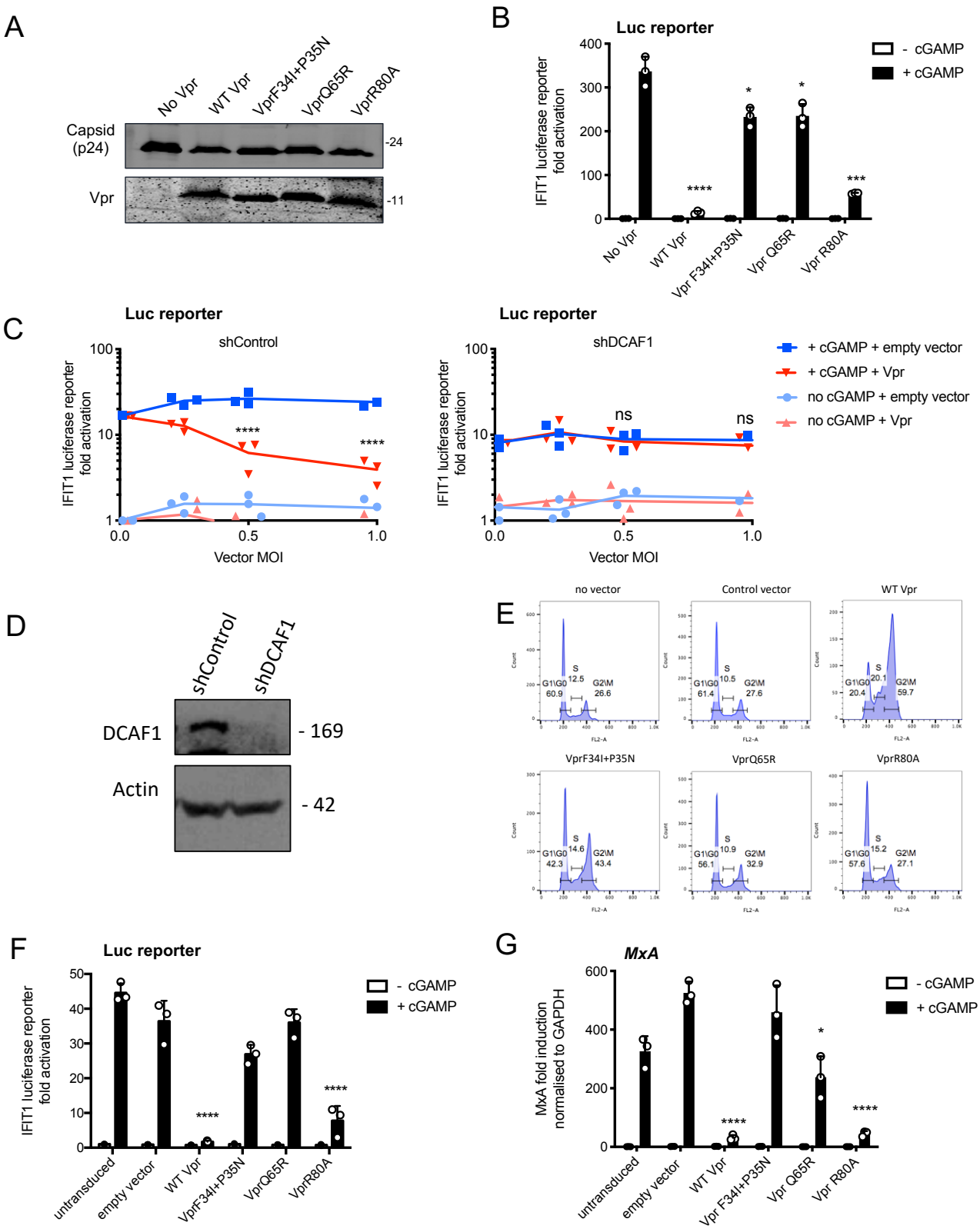

Figure 3 Vpr inhibition of innate immune activation is dependent on DCAF1 but independent of cell cycle arrest

(A) Immunoblot detecting p24 (capsid) and Vpr in pelleted VLPs. Size markers in kDa are indicated on the right.

773 (B) Fold induction of IFIT1-Luc after activation of STING by cGAMP (5 µg/ml) and infection with
774 VLP bearing WT or mutant Vpr, or lacking Vpr (1 RT U/ml) in IFIT1-Luc reporter THP1 cells.
775
776 (C) Fold induction of IFIT1-Luc after activation of STING by cGAMP (5 µg/ml) in cells expressing
777 Vpr from a lentiviral vector, or empty vector, or in untransduced IFIT1-Luc reporter THP1 cells
778 expressing a control, or a DCAF1 targeting shRNA. Data combined from three independent
779 experiments are shown.
780
781 (D) Immunoblot detecting DCAF1, or actin as a loading control, from extracted THP1 cells
782 expressing a control, or DCAF1-targeting, shRNA. Size markers are shown in kDa on the right.
783
784 (E) Flow cytometry plots showing cell cycle phases of THP1 cells transduced with an empty
785 vector, WT Vpr, or mutant Vpr, encoding vector (MOI 1) or left untransduced as a control and
786 stained with propidium iodide to label DNA. Percentage cells in each cell cycle stage are shown.
787
788 (F) Fold induction of IFIT1-Luc after activation of STING by cGAMP (5 µg/ml) in cells expressing
789 WT, or mutant, Vpr from a lentiviral vector (MOI 1), or empty vector (MOI 1) or in untransduced
790 IFIT1-Luc reporter THP1 cells.
791
792 (G) Fold induction of *MxA* mRNA after activation of STING by cGAMP (5 µg/ml) in cells
793 expressing WT, or mutant, Vpr from a lentiviral vector (MOI 1), or after transduction by empty
794 vector (MOI 1) or in untransduced THP1 cells.
795
796 Data are expressed as means ± SD (n = 3). Two-way ANOVA test: * ($p<0.05$), ** ($p<0.01$), ***
797 ($p<0.001$), **** ($p<0.0001$) compared to no Vpr or empty vector controls. Data are representative
798 of three (B-D, F) or two (A, E, G) independent experiments.
799

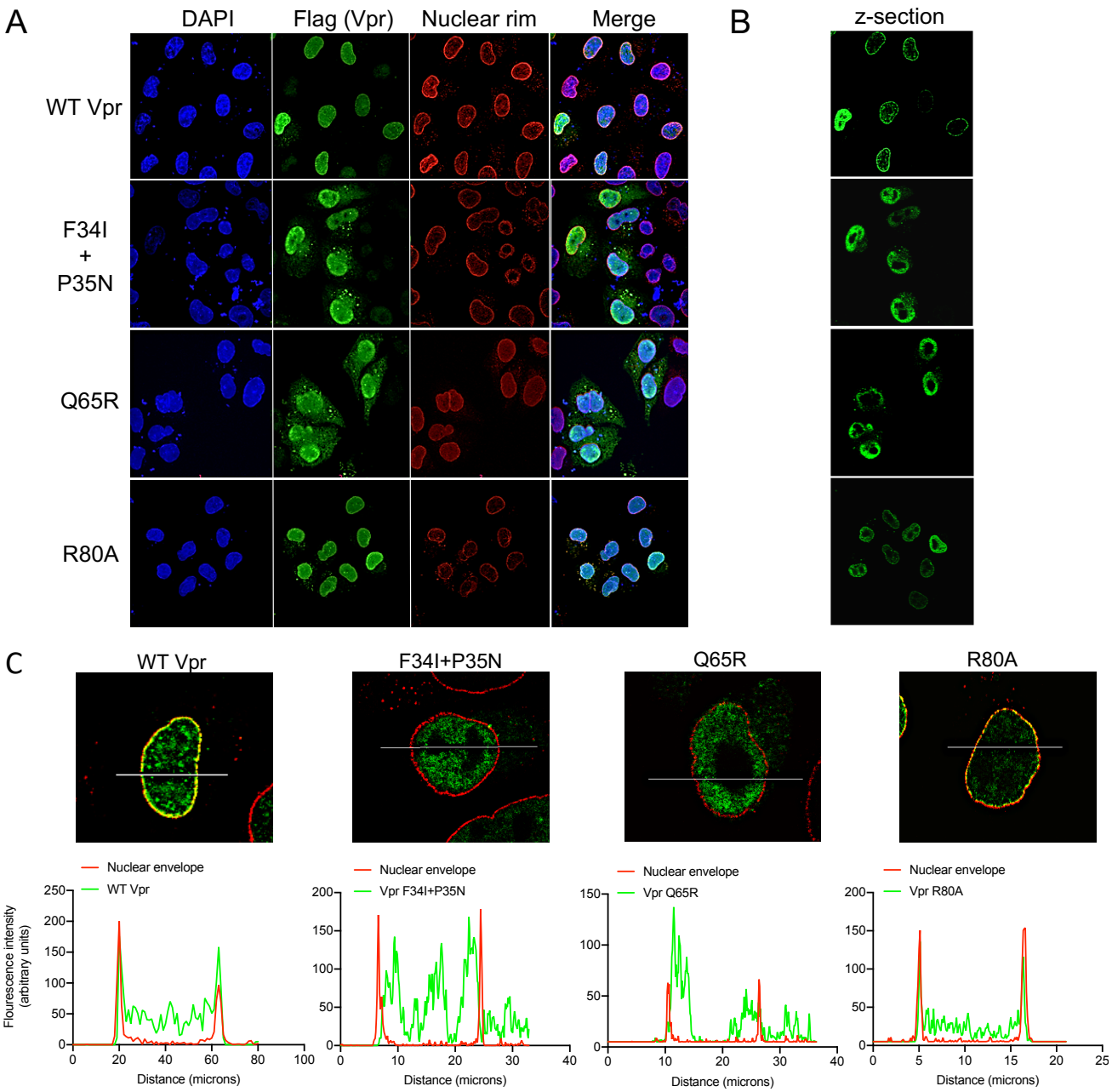

Figure 4 Wild Type Vpr, but not sensing antagonism inactive Vpr mutants, localise to nuclear pores

(A) Immunofluorescence confocal projections of HeLa cells transfected with Flag-tagged WT, or mutant, Vpr encoded by pcDNA3.1 plasmid (50 ng) and stained using antibodies detecting the Flag-tag (green) or nuclear pore complex (mab414) (red). 4′,6-Diamidine-2′-phenylindole dihydrochloride (DAPI) stains nuclear DNA (Blue).

(B) Selected confocal images (z-section) of cells in (A) showing effect of Vpr mutation on Vpr colocalization with mab414 nuclear pore staining.

(C) Assessment of colocalization of Vpr with mab414 nuclear pore staining.

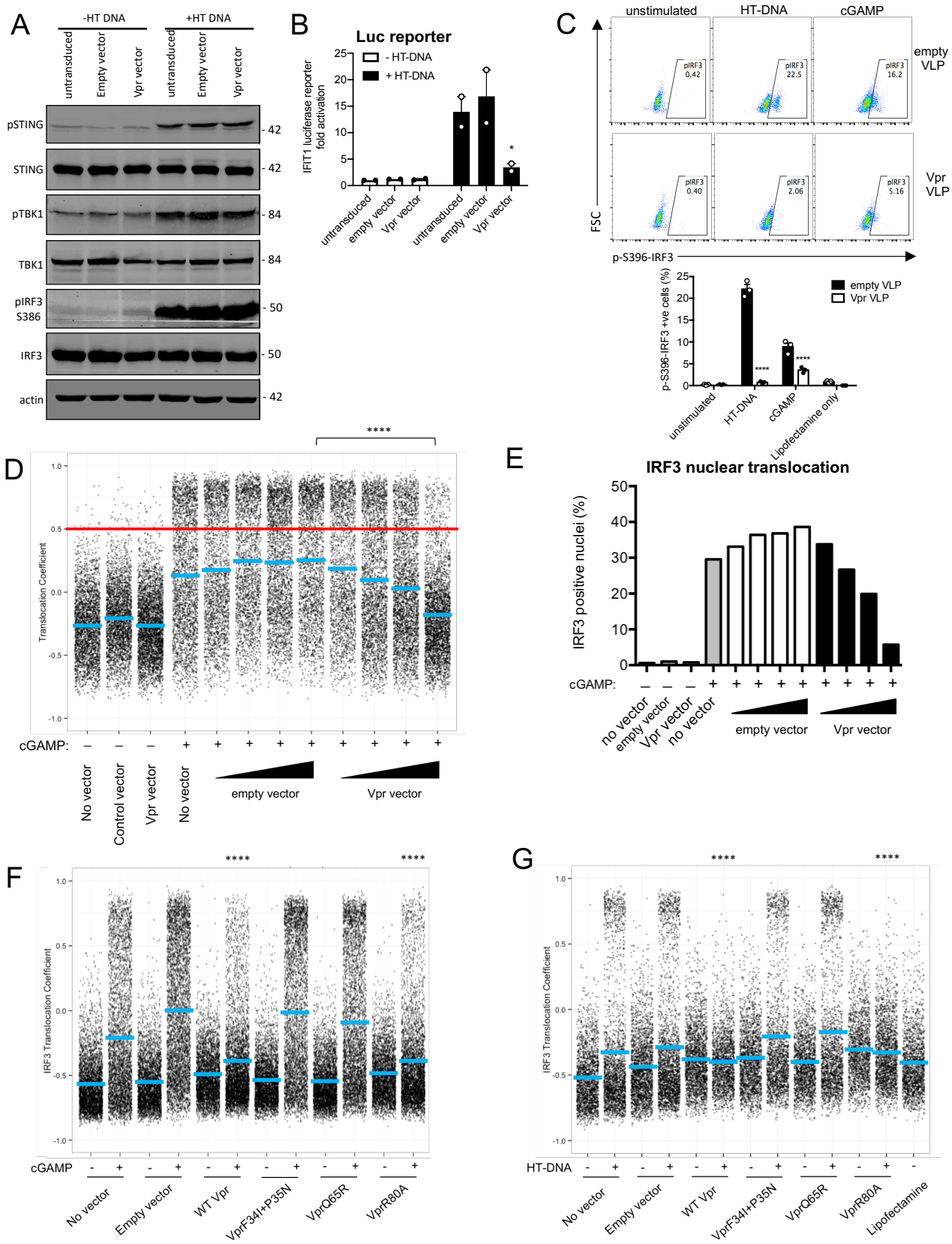

Figure 5 Vpr inhibits IRF3 nuclear translocation

(A) Immunoblot detecting Phospho-STING (Ser366), total STING, phospho-TBK1 (Ser172), total TBK1, phospho-IRF3 (Ser386), total IRF3, or actin as a loading control, from extracted THP1

821 cells expressing Vpr from a lentiviral vector (MOI 1), or after empty vector transduction, or left
822 untransduced as a control and transfected with HT-DNA (5 µg/ml) or left untransfected as a
823 control. Size markers are shown in kDa.
824
825 (B) Mean fold induction of IFIT1-Luc in cells from Figure 5A and Figure S5B transduced with
826 empty vector or Vpr vector and transfected with HT-DNA (5 µg/ml) or left untreated as a control.
827
828 (C) Flow cytometry plot (forward scatter vs pIRF3-S396 fluorescence) of THP1 cells infected with
829 Vpr bearing virus-like particles (1 RT U/ml), or Vpr free particles, and stimulated with cGAMP (5
830 µg/ml) or HT-DNA transfection (5 µg/ml). Bottom panel shows the flow cytometry plot data as a
831 bar graph, plotting pIRF3-S396 positive cells in each case.
832
833 (D) Single cell immunofluorescence measurement of IRF3 nuclear translocation in PMA
834 differentiated THP1 cells treated with cGAMP, or left untreated, and infected with empty vector,
835 Vpr encoding vector or left uninfected. Red line shows the translocation coefficient threshold.
836 Blue lines represent mean translocation coefficient.
837
838 (E) Percentage of cells in Figure 5D with IRF3 translocation coefficient greater than 0.5 (above
839 red line).
840
841 (F) Single cell immunofluorescence measurement of IRF3 nuclear translocation in PMA
842 differentiated THP1 cells stimulated with cGAMP (5 µg/ml), or left unstimulated, and infected with
843 empty vector, WT or mutant Vpr encoding vector (1 RT U/ml) or left uninfected.
844
845 (G) Single cell immunofluorescence measurement of IRF3 nuclear translocation in PMA
846 differentiated THP1 cells transfected with HT-DNA (5 µg/ml), or left untransfected, and infected
847 with empty vector, WT or mutant Vpr encoding vector (1 RT U/ml) or left uninfected.
848
849 Data in B is expressed as means ± SEM (n = 2). Data is analysed using two-way ANOVA: *
850 ($p<0.05$), ** ($p<0.01$), *** ($p<0.001$), **** ($p<0.0001$) compared to empty vector or empty VLP.
851 Data are representative of three (C–G) or two (A, B) independent experiments.
852

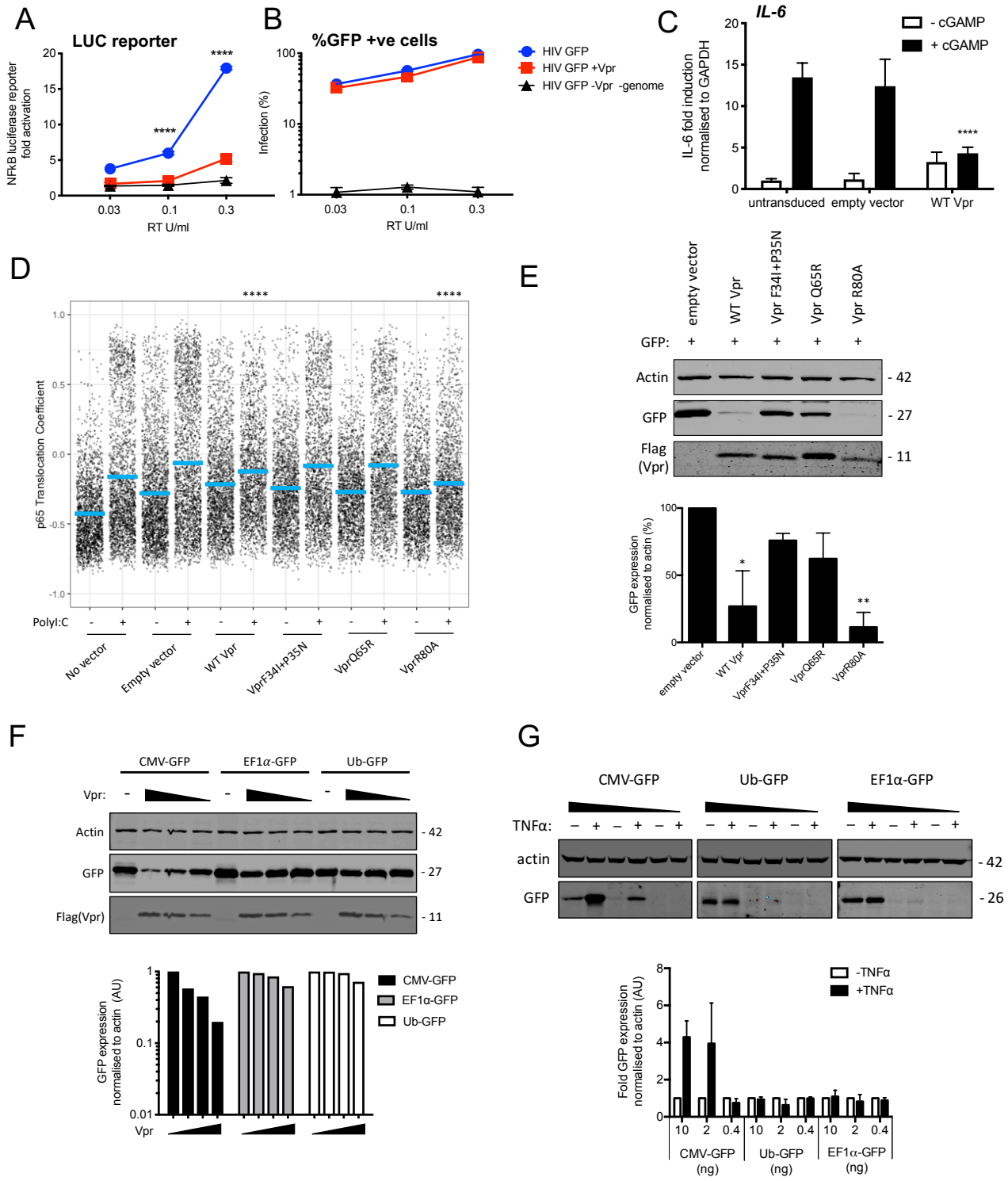

Figure 6 Vpr inhibits NF-κB p65 nuclear translocation and NF-κB sensitive plasmid expression

(A) Fold induction of NF-κB-Luc after infection of THP1 cells with HIV-GFP -Vpr, HIV-GFP +Vpr, or HIV-GFP -Vpr lacking genome, at the indicated doses.

(B) Percentage of THP1 cells in (A) infected by HIV-GFP -Vpr, HIV-GFP +Vpr, or HIV-GFP -Vpr lacking genome at the indicated doses.

(C) Fold induction of *IL-6* after activation of STING by cGAMP (5 µg/ml) in cells expressing Vpr from a lentiviral vector (MOI 1), or after empty vector transduction or in untransduced THP1 cells.

(D) Single cell immunofluorescence measurement of NF-kB (p65) nuclear translocation in PMA differentiated THP1 cells transfected with Poly I:C (50 ng/ml), or left untreated, and infected with empty vector (1 RT U/ml), Vpr vector (1 RT U/ml) or left uninfected.

(E) Immunoblot detecting Flag-Vpr, GFP, or actin as a loading control, from HEK293T cells transfected with 50 ng of empty vector, Flag-tagged WT Vpr vector, or Flag-tagged mutant Vpr vector, and CMV-GFP vector (50 ng). Size markers are shown in kDa. GFP expression from two independent immunoblots quantified by densitometry is shown in the lower panel.

(F) Immunoblot detecting Flag-Vpr, GFP, or actin as a loading control, from HEK293T cells transfected with empty vector (200 ng) or Vpr vector (50ng, 100ng, 200ng) and CMV-GFP, EF1α-GFP or Ub-GFP plasmids (50 ng). Size markers are shown in kDa. GFP expression quantified by densitometry is shown in the lower panel.

(G) Immunoblot detecting GFP, or actin as a loading control, from HEK293T cells transfected with CMV-GFP, EF1α-GFP or Ub-GFP plasmids (10 ng, 2 ng, 0.4 ng) and stimulated with TNFα (200 ng/ml) or left unstimulated. Size markers are shown in kDa. GFP expression, from two independent immunoblots, quantified by densitometry, is shown in the lower panel.

Data in (A, B, C) is expressed as mean ± SD (n = 3). Data in (E, F, G) is expressed as mean ± SD (n=2). Two-way ANOVA: * ($p<0.05$), ** ($p<0.01$), *** ($p<0.001$), **** ($p<0.0001$) compared to empty vector or HIV GFP+Vpr.

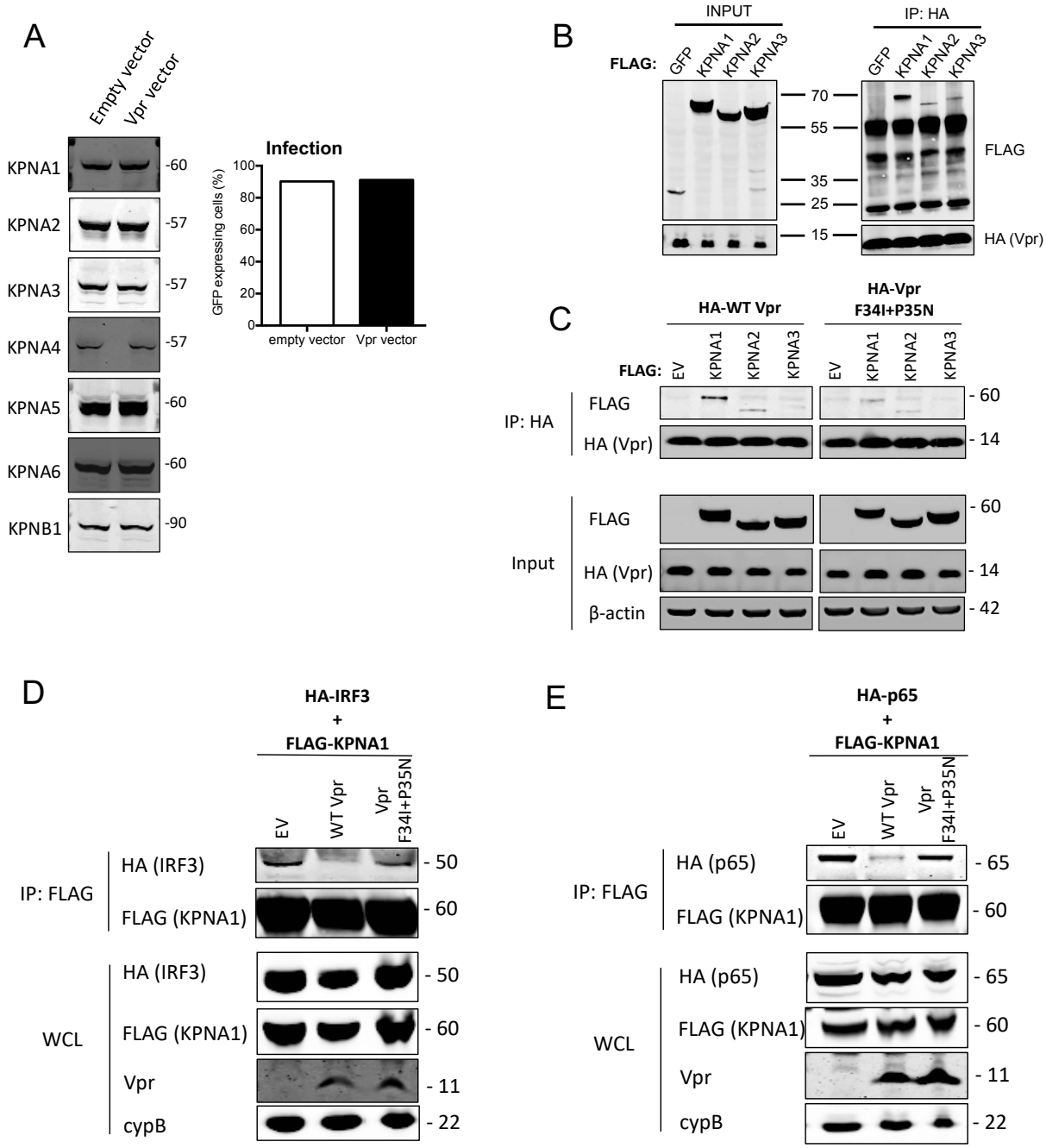

Figure 7 HIV-1 Vpr interacts with karyopherins and inhibits IRF3/NF-κB(p65) recruitment to KPNA1

(A) Immunoblot detecting KPNA1-6 or KPNB1 from extracted HEK293T cells infected with empty vector, or Vpr encoding vector at a dose of 0.05 RT U/ml (MOI=2). Size markers are shown in kDa. Percentage infection by Vpr encoding or empty HIV-1 vector is shown on the right.

(B) Co-immunoprecipitation of Flag-KPNA1-3 and HA-Vpr. Input shows immunoblot detecting extracted HEK293T whole cell lysates expressing flag-KPNA1-3, flag-GFP and HA-Vpr before immunoprecipitation. Co-immunoprecipitation precipitates Vpr with HA-beads and detects Flag-KPNA1-3.

(C) Co-immunoprecipitation of Flag-KPNA1-3 and WT HA-Vpr or HA-Vpr F34I+P35N. Input shows immunoblots detecting HA-Vpr or Flag-KPNA1-3 in extracted HEK293T whole cell lysates (WCL) before immunoprecipitation. β-Actin is detected as a loading control. Co-immunoprecipitation precipitates Vpr with HA-beads and detects Flag-KPNA1-3.

908
909 (D) Co-immunoprecipitation of HA-IRF3 and Flag-KPNA1 in the presence and absence of WT
910 Vpr or Vpr F34I+P35N to detect competition between Vpr and IRF3 for KPNA1. Input shows
911 immunoblots detecting HA-IRF3 or Flag-KPNA1 or Vpr in extracted HEK293T whole cell lysates
912 (WCL) before immunoprecipitation. CypB is detected as a loading control. Co-
913 immunoprecipitation precipitates KPNA1 with Flag-beads and detects HA-IRF3 in the presence
914 and absence of WT Vpr or Vpr F34I+P35N.
915
916 (E) Co-immunoprecipitation of HA-p65 and Flag-KPNA1 in the presence and absence of WT Vpr
917 or Vpr F34I+P35N to detect competition between Vpr and p65 for KPNA1. Input shows
918 immunoblots detecting HA-p65 or Flag-KPNA1 or Vpr in extracted HEK293T whole cell lysates
919 (WCL) before immunoprecipitation. CypB is detected as a loading control. Co-
920 immunoprecipitation precipitates KPNA1 with Flag-beads and detects HA-p65 in the presence
921 and absence of WT Vpr or Vpr F34I+P35N.
922

923 **References**

924 Ahn, J., Vu, T., Novince, Z., Guerrero-Santoro, J., Rapic-Otrin, V., & Gronenborn, A. M. (2010). HIV-1
925 Vpr loads uracil DNA glycosylase-2 onto DCAF1, a substrate recognition subunit of a cullin 4A-
926 RING E3 ubiquitin ligase for proteasome-dependent degradation. *Journal of Biological*
927 *Chemistry*, *258*(48), 37333–37341. https://doi.org/10.1074/jbc.M110.133181
928 Ali, A., Ng, H. L., Blankson, J. N., Burton, D. R., Buckheit, R. W. 3rd, Moldt, B., Fulcher, J. A.,
929 Ibarrondo, F. J., Anton, P. A., & Yang, O. O. (2018). Highly Attenuated Infection With a Vpr-
930 Deleted Molecular Clone of Human Immunodeficiency Virus-1. *The Journal of Infectious*
931 *Diseases*, *218*(9), 1447–1452. https://doi.org/10.1093/infdis/jiy346
932 Andrejeva, J., Childs, K. S., Young, D. F., Carlos, T. S., Stock, N., Goodbourn, S., & Randall, R. E.
933 (2004). The V proteins of paramyxoviruses bind the IFN-inducible RNA helicase, mda-5, and
934 inhibit its activation of the IFN-β promoter. *Proceedings of the National Academy of Sciences of*
935 *the United States of America*, *101*(49), 17264–17269. https://doi.org/10.1073/pnas.0407639101
936 Bachand, F., Yao, X.-J., Hrimech, M., Rougeau, N., & Cohen, É. A. (1999). Incorporation of Vpr into
937 human immunodeficiency virus type 1 requires a direct interaction with the p6 domain of the p55
938 Gag precursor. *Journal of Biological Chemistry*, *274*(13), 9083–9091.
939 https://doi.org/10.1074/jbc.274.13.9083
940 Bejarano, D. A., Peng, K., Laketa, V., Börner, K., Jost, K. L., Lucic, B., Glass, B., Lusic, M., Müller, B.,
941 & Kräusslich, H.-G. (2019). HIV-1 nuclear import in macrophages is regulated by CPSF6-capsid
942 interactions at the nuclear pore complex. *ELife*, *8*, e41800. https://doi.org/10.7554/elife.41800
943 Belzile, J. P., Abrahamyan, L. G., Gérard, F. C. A., Rougeau, N., & Cohen, É. A. (2010). Formation of
944 mobile chromatin-associated nuclear foci containing HIV-1 Vpr and VPRBP is critical for the
945 induction of G2 cell cycle arrest. *PLoS Pathogens*, *6*(9), e1001080.
946 https://doi.org/10.1371/journal.ppat.1001080
947 Berger, G., Lawrence, M., Hué, S., & Neil, S. J. D. (2015). G2/M cell cycle arrest correlates with
948 primate lentiviral Vpr interaction with the SLX4 complex. *Journal of Virology*, *89*(1), 230–240.
949 https://doi.org/10.1128/JVI.02307-14
950 Burdick, R. C., Delviks-Frankenberry, K. A., Chen, J., Janaka, S. K., Sastri, J., Hu, W. S., & Pathak,
951 V. K. (2017). Dynamics and regulation of nuclear import and nuclear movements of HIV-1
952 complexes. *PLoS Pathogens*, *13*(8), e1006570. https://doi.org/10.1371/journal.ppat.1006570
953 Chen, W., Srinath, H., Lam, S. S., Schiffer, C. A., Royer, W. E., & Lin, K. (2008). Contribution of
954 Ser386 and Ser396 to Activation of Interferon Regulatory Factor 3. *Journal of Molecular Biology*,
955 *379*(2), 251–260. https://doi.org/10.1016/j.jmb.2008.03.050
956 DeMeritt, I. B., Milford, L. E., & Yurochko, A. D. (2004). Activation of the NF-κB Pathway in Human
957 Cytomegalovirus-Infected Cells Is Necessary for Efficient Transactivation of the Major
958 Immediate-Early Promoter. *Journal of Virology*, *78*(9), 498–507.
959 https://doi.org/10.1128/jvi.78.9.4498-4507.2004
960 Douglas Dedera, Wen Hu, Nancy Vander, Heyden, L. R. (1989). Viral Protein R of Human
961 Immunodeficiency Virus Types 1 and 2 Is Despensable for Replication and Cytopathogenicity in
962 Lymphoid Cells. *Journal of Virology*, *63*(7), 3205–3208. https://doi.org/10.1007/BF02297789

963 Fagerlund, R., Kinnunen, L., Kohler, M., Julkunen, I., & Melen, K. (2005). NF-{kappa}B is transported
964 into the nucleus by importin {alpha}3 and importin {alpha}4. *The Journal of Biological Chemistry*,
965 *280*(16), 15942–15951. https://doi.org/10.1074/jbc.M500814200
966 Fagerlund, R., Melén, K., Cao, X., & Julkunen, I. (2008). NF-κB p52, RelB and c-Rel are transported
967 into the nucleus via a subset of importin α molecules. *Cellular Signalling*, *20*(8), 1442–1451.
968 https://doi.org/10.1016/j.cellsig.2008.03.012
969 Fang, R., Wang, C., Jiang, Q., Lv, M., Gao, P., Yu, X., Mu, P., Zhang, R., Bi, S., Feng, J.-M., & Jiang,
970 Z. (2017). NEMO–IKKβ Are Essential for IRF3 and NF-κB Activation in the cGAS–STING
971 Pathway. *The Journal of Immunology*, *199*(9), 3222–3233.
972 https://doi.org/10.4049/jimmunol.1700699
973 Fischer, W., Ganusov, V. V, Giorgi, E. E., Hraber, P. T., Keele, B. F., Leitner, T., Han, C. S.,
974 Gleasner, C. D., Green, L., Lo, C.-C., Nag, A., Wallstrom, T. C., Wang, S., McMichael, A. J.,
975 Haynes, B. F., Hahn, B. H., Perelson, A. S., Borrow, P., Shaw, G. M., … Korber, B. T. (2010).
976 Transmission of single HIV-1 genomes and dynamics of early immune escape revealed by ultra-
977 deep sequencing. *PloS One*, *5*(8), e12303–e12303.
978 https://doi.org/10.1371/journal.pone.0012303
979 Foster, T L, Wilson, H., Iyer, S. S., Coss, K., Doores, K., Smith, S., Kellam, P., Finzi, A., Borrow, P.,
980 Hahn, B. H., & Neil, S. J. D. (2016). Resistance of Transmitted Founder HIV-1 to IFITM-
981 Mediated Restriction. *Cell Host and Microbe*, *20*(4), 429–442.
982 https://doi.org/10.1016/j.chom.2016.08.006
983 Foster, Toshana L, Pickering, S., & Neil, S. J. D. (2017). Inhibiting the Ins and Outs of HIV
984 Replication: Cell-Intrinsic Antiretroviral Restrictions at the Plasma Membrane. *Frontiers in*
985 *Immunology*, *8*, 1853. https://doi.org/10.3389/fimmu.2017.01853
986 Fouchier, R. A. M., Meyer, B. E., Simon, J. H. M., Fischer, U., Albright, A. V, González-Scarano, F., &
987 Malim, M. H. (1998). Interaction of the human immunodeficiency virus type 1 Vpr protein with the
988 nuclear pore complex. *Journal of Virology*, *72*(7), 6004–6013.
989 https://www.scopus.com/inward/record.uri?eid=2-s2.0-
990 0031799691&partnerID=40&md5=95c739e3621c2e60756318f4b498b0e9
991 Francis, A. C., Marin, M., Shi, J., Aiken, C., & Melikyan, G. B. (2016). Time-Resolved Imaging of
992 Single HIV-1 Uncoating In Vitro and in Living Cells. *PLoS Pathogens*, *12*(6), e1005709.
993 https://doi.org/10.1371/journal.ppat.1005709
994 Gagne, B., Tremblay, N., Park, A. Y., Baril, M., & Lamarre, D. (2017). Importin beta1 targeting by
995 hepatitis C virus NS3/4A protein restricts IRF3 and NF-kappaB signaling of IFNB1 antiviral
996 response. *Traffic (Copenhagen, Denmark)*, *18*(6), 362–377. https://doi.org/10.1111/tra.12480
997 Gao, D., Wu, J., Wu, Y.-T., Du, F., Aroh, C., Yan, N., Sun, L., & Chen, Z. J. (2013). Cyclic GMP-AMP
998 synthase is an innate immune sensor of HIV and other retroviruses. *Science*, *341*(6148), 903–
999 906. https://doi.org/10.1126/science.1240933
1000 Gaynor, E. M., & Chen, I. S. Y. (2001). Analysis of apoptosis induced by HIV-1 Vpr and examination
1001 of the possible role of the hHR23A protein. *Experimental Cell Research*, *267*(2), 243–257.
1002 https://doi.org/10.1006/excr.2001.5247

1003 Goujon, C., Moncorgé, O., Bauby, H., Doyle, T., Ward, C. C., Schaller, T., Hué, S., Barclay, W. S.,
1004 Schulz, R., & Malim, M. H. (2013). Human MX2 is an interferon-induced post-entry inhibitor of
1005 HIV-1 infection. *Nature*, *502*(7472), 559–562. https://doi.org/10.1038/nature12542
1006 Greenwood, E. J. D., Williamson, J. C., Sienkiewicz, A., Naamati, A., Matheson, N. J., & Lehner, P. J.
1007 (2019). Promiscuous Targeting of Cellular Proteins by Vpr Drives Systems-Level Proteomic
1008 Remodeling in HIV-1 Infection. *Cell Reports*, *27*(5), 1579-1596.e7.
1009 https://doi.org/10.1016/j.celrep.2019.04.025
1010 Griffin, G. E., Leung, K., Folks, T. M., Kunkel, S., & Nabel, G. J. (1989). Activation of HIV gene
1011 expression during monocyte differentiation by induction of NF-kB. *Nature*, *339*(6219), 70–73.
1012 https://doi.org/10.1038/339070a0
1013 Gulen, M. F., Koch, U., Haag, S. M., Schuler, F., Apetoh, L., Villunger, A., Radtke, F., & Ablasser, A.
1014 (2017). Signalling strength determines proapoptotic functions of STING. *Nature*
1015 *Communications*. https://doi.org/10.1038/s41467-017-00573-w
1016 Hattori, N., Michaels, F., Fargnoli, K., Marcon, L., Gallo, R. C., & Franchini, G. (1990). The human
1017 immunodeficiency virus type 2 vpr gene is essential for productive infection of human
1018 macrophages. *Proceedings of the National Academy of Sciences*, *87*(20), 8080–8084.
1019 https://doi.org/10.1073/pnas.87.20.8080
1020 Iyer, S. S., Bibollet-Ruche, F., Sherrill-Mix, S., Learn, G. H., Plenderleith, L., Smith, A. G., Barbian, H.
1021 J., Russell, R. M., Gondim, M. V. P., Bahari, C. Y., Shaw, C. M., Li, Y., Decker, T., Haynes, B.
1022 F., Shaw, G. M., Sharp, P. M., Borrow, P., & Hahn, B. H. (2017). Resistance to type 1
1023 interferons is a major determinant of HIV-1 transmission fitness. *Proceedings of the National*
1024 *Academy of Sciences of the United States of America*, *114*(4), E590–E599.
1025 https://doi.org/10.1073/pnas.1620144114
1026 Jacques, D. A., McEwan, W. A., Hilditch, L., Price, A. J., Towers, G. J., & James, L. C. (2016). HIV-1
1027 uses dynamic capsid pores to import nucleotides and fuel encapsidated DNA synthesis. *Nature*,
1028 *536*(7616), 349–353. https://doi.org/10.1038/nature19098
1029 Jimenez-Guardeño, J. M., Apolonia, L., Betancor, G., & Malim, M. H. (2019). Immunoproteasome
1030 activation enables human TRIM5α restriction of HIV-1. *Nature Microbiology*, *4*(6), 933–940.
1031 https://doi.org/10.1038/s41564-019-0402-0
1032 Kane, M., Yadav, S. S., Bitzegeio, J., Kutluay, S. B., Zang, T., Wilson, S. J., Schoggins, J. W., Rice,
1033 C. M., Yamashita, M., Hatziioannou, T., & Bieniasz, P. D. (2013). MX2 is an interferon-induced
1034 inhibitor of HIV-1 infection. *Nature*, *502*(7472), 563–566. https://doi.org/10.1038/nature12653
1035 Kumar, K. P., McBride, K. M., Weaver, B. K., Dingwall, C., & Reich, N. C. (2002). Regulated Nuclear-
1036 Cytoplasmic Localization of Interferon Regulatory Factor 3, a Subunit of Double-Stranded RNA-
1037 Activated Factor 1. *Molecular and Cellular Biology*, *20*(11), 4159–4168.
1038 https://doi.org/10.1128/mcb.20.11.4159-4168.2000
1039 Laguette, N., Brégnard, C., Hue, P., Basbous, J., Yatim, A., Larroque, M., Kirchhoff, F., Constantinou,
1040 A., Sobhian, B., & Benkirane, M. (2014). Premature activation of the slx4 complex by vpr
1041 promotes g2/m arrest and escape from innate immune sensing. *Cell*, *156*(1–2), 134–145.
1042 https://doi.org/10.1016/j.cell.2013.12.011

1043 Lahaye, X., Satoh, T., Gentili, M., Cerboni, S., Conrad, C., Hurbain, I., ElMarjou, A., Lacabaratz, C.,
1044 Lelièvre, J.-D., & Manel, N. (2013). The Capsids of HIV-1 and HIV-2 Determine Immune
1045 Detection of the Viral cDNA by the Innate Sensor cGAS in Dendritic Cells. *Immunity*, *39*(6),
1046 1132–1142. https://doi.org/10.1016/j.immuni.2013.11.002
1047 Lahouassa, H., Blondot, M.-L., Chauveau, L., Chougui, G., Morel, M., Leduc, M., Guillonneau, F.,
1048 Ramirez, B. C., Schwartz, O., & Margottin-Goguet, F. (2016). HIV-1 Vpr degrades the HLTF
1049 DNA translocase in T cells and macrophages. *Proceedings of the National Academy of*
1050 *Sciences of the United States of America*, *113*(19), 5311–5316.
1051 https://doi.org/10.1073/pnas.1600485113
1052 Le Rouzic, E., Mousnier, A., Rustum, C., Stutz, F., Hallberg, E., Dargemont, C., & Benichou, S.
1053 (2002). Docking of HIV-1 vpr to the nuclear envelope is mediated by the interaction with the
1054 nucleoporin hCG1. *Journal of Biological Chemistry*, *277*(47), 45091–45098.
1055 https://doi.org/10.1074/jbc.M207439200
1056 Liang, P., Zhang, H., Wang, G., Li, S., Cong, S., Luo, Y., & Zhang, B. (2013). KPNB1, XPO7 and
1057 IPO8 mediate the translocation ofNF-kappaB/p65 into the nucleus. *Traffic (Copenhagen,*
1058 *Denmark)*, *14*(11), 1132–1143. https://doi.org/10.1111/tra.12097
1059 Lin, R., Mamane, Y., & Hiscott, J. (1999). Structural and functional analysis of interferon regulatory
1060 factor 3: localization of the transactivation and autoinhibitory domains. *Molecular and Cellular*
1061 *Biology*, *19*(4), 2465–2474.
1062 Liu, S., Cai, X., Wu, J., Cong, Q., Chen, X., Li, T., Du, F., Ren, J., Wu, Y. T., Grishin, N. V., & Chen,
1063 Z. J. (2015). Phosphorylation of innate immune adaptor proteins MAVS, STING, and TRIF
1064 induces IRF3 activation. *Science*, *13*(347), 2630. https://doi.org/10.1126/science.aaa2630
1065 Liu, X., Guo, H., Wang, H., Markham, R., Wei, W., & Yu, X. F. (2015). HIV-1 Vpr suppresses the
1066 cytomegalovirus promoter in a CRL4(DCAF1) E3 ligase independent manner. *Biochemical and*
1067 *Biophysical Research Communications*, *459*(2), 214–219.
1068 https://doi.org/10.1016/j.bbrc.2015.02.060
1069 Mankan, A. K., Schmidt, T., Chauhan, D., Goldeck, M., Höning, K., Gaidt, M., Kubarenko, A. V,
1070 Andreeva, L., Hopfner, K., & Hornung, V. (2014). Cytosolic RNA:DNA hybrids activate the cGAS
1071 –STING axis. *The EMBO Journal*, *33*(24), 2937–2946. https://doi.org/10.15252/embj.201488726
1072 Matsuda, T., & Cepko, C. L. (2004). Electroporation and RNA interference in the rodent retina in vivo
1073 and in vitro. *Proceedings of the National Academy of Sciences of the United States of America*,
1074 *101*(1), 16–22. https://doi.org/10.1073/pnas.2235688100
1075 Mesika, A., Grigoreva, I., Zohar, M., & Reich, Z. (2001). A regulated, NFκB-assisted import of plasmid
1076 DNA into mammalian cell nuclei. *Molecular Therapy*, *3*(5Pt1), 653–657.
1077 https://doi.org/10.1006/mthe.2001.0312
1078 Morellet, N., Bouaziz, S., Petitjean, P., & Roques, B. P. (2003). NMR structure of the HIV-1 regulatory
1079 protein VPR. *Journal of Molecular Biology*, *285*(5), 2105–2117. https://doi.org/10.1016/S0022-
1080 2836(03)00060-3
1081 Mori, M., Yoneyama, M., Ito, T., Takahashi, K., Inagaki, F., & Fujita, T. (2004). Identification of Ser-
1082 386 of Interferon Regulatory Factor 3 as Critical Target for Inducible Phosphorylation That

1083 Determines Activation. *Journal of Biological Chemistry*, *279*(11), 9698–9702.
1084 https://doi.org/10.1074/jbc.M310616200
1085 Nitahara-Kasahara, Y., Kamata, M., Yamamoto, T., Zhang, X., Miyamoto, Y., Muneta, K., Iijima, S.,
1086 Yoneda, Y., Tsunetsugu-Yokota, Y., & Aida, Y. (2007). Novel Nuclear Import of Vpr Promoted by
1087 Importin Is Crucial for Human Immunodeficiency Virus Type 1 Replication in Macrophages.
1088 *Journal of Virology*, *81*(10), 5284–5293. https://doi.org/10.1128/jvi.01928-06
1089 Pallett, M. A., Ren, H., Zhang, R.-Y., Scutts, S. R., Gonzalez, L., Zhu, Z., Maluquer de Motes, C., &
1090 Smith, G. L. (2019). Vaccinia Virus BBK E3 Ligase Adaptor A55 Targets Importin-Dependent
1091 NF-κB Activation and Inhibits CD8 + T-Cell Memory. *Journal of Virology*, *93*(10), e00051-19.
1092 https://doi.org/10.1128/jvi.00051-19
1093 Rasaiyaah, J., Tan, C. P., Fletcher, A. J., Price, A. J., Blondeau, C., Hilditch, L., Jacques, D. A.,
1094 Selwood, D. L., James, L. C., Noursadeghi, M., & Towers, G. J. (2013). HIV-1 evades innate
1095 immune recognition through specific cofactor recruitment. *Nature*, *503*(7476), 402–405.
1096 https://doi.org/10.1038/nature12769
1097 Rehwinkel, J., Tan, C. P., Goubau, D., Schulz, O., Pichlmair, A., Bier, K., Robb, N., Vreede, F.,
1098 Barclay, W., Fodor, E., & Reis e Sousa, C. (2010). RIG-I Detects Viral Genomic RNA during
1099 Negative-Strand RNA Virus Infection. *Cell*, *140*(3), 397–408.
1100 https://doi.org/10.1016/j.cell.2010.01.020
1101 Schaller, T., Ocwieja, K. E., Rasaiyaah, J., Price, A. J., Brady, T. L., Roth, S. L., Hué, S., Fletcher, A.
1102 J., Lee, K., KewalRamani, V. N., Noursadeghi, M., Jenner, R. G., James, L. C., Bushman, F. D.,
1103 & Towers, G. J. (2011). HIV-1 capsid-cyclophilin interactions determine nuclear import pathway,
1104 integration targeting and replication efficiency. *PLoS Pathogens*, *7*(12).
1105 https://doi.org/10.1371/journal.ppat.1002439
1106 Schirrmacher, V. (2015). Signaling through RIG-I and type I interferon receptor: Immune activation by
1107 Newcastle disease virus in man versus immune evasion by Ebola virus (Review). *International*
1108 *Journal of Molecular Medicine*, *36*(1), 3–10. https://doi.org/10.3892/ijmm.2015.2213
1109 Schwefel, D., Groom, H. C. T., Boucherit, V. C., Christodoulou, E., Walker, P. A., Stoye, J. P., Bishop,
1110 K. N., & Taylor, I. A. (2014). Structural basis of lentiviral subversion of a cellular protein
1111 degradation pathway. *Nature*. https://doi.org/10.1038/nature12815
1112 Servant, M. J., Grandvaux, N., TenOever, B. R., Duguay, D., Lin, R., & Hiscott, J. (2003).
1113 Identification of the minimal phosphoacceptor site required for in vivo activation of interferon
1114 regulatory factor 3 in response to virus and double-stranded RNA. *Journal of Biological*
1115 *Chemistry*, *278*(11), 9441–9447. https://doi.org/10.1074/jbc.M209851200
1116 Shaw, G. M., & Hunter, E. (2012). HIV transmission. *Cold Spring Harbor Perspectives in Medicine*,
1117 *2*(11), a006965. https://doi.org/10.1101/cshperspect.a006965
1118 Stacey, A. R., Norris, P. J., Qin, L., Haygreen, E. A., Taylor, E., Heitman, J., Lebedeva, M., DeCamp,
1119 A., Li, D., Grove, D., Self, S. G., & Borrow, P. (2009). Induction of a striking systemic cytokine
1120 cascade prior to peak viremia in acute human immunodeficiency virus type 1 infection, in
1121 contrast to more modest and delayed responses in acute hepatitis B and C virus infections.
1122 *Journal of Virology*, *83*(8), 3719–3733. https://doi.org/10.1128/JVI.01844-08

1123 Suhara, W., Yoneyama, M., Iwamura, T., Yoshimura, S., Tamura, K., Namiki, H., Aimoto, S., & Fujita,
1124 T. (2000). Analyses of virus-induced homomeric and heteromeric protein associations between
1125 IRF-3 and coactivator CBP/p300. *Journal of Biochemistry*, *128*(2), 301–307.
1126 https://doi.org/10.1093/oxfordjournals.jbchem.a022753
1127 Sumner, R.P., Thorne, L. G., Fink, D. L., Khan, H., Milne, R. S., & Towers, G. J. (2017). Are evolution
1128 and the intracellular innate immune system key determinants in HIV transmission? *Frontiers in*
1129 *Immunology*, *8*(OCT). https://doi.org/10.3389/fimmu.2017.01246
1130 Sumner, Rebecca P, Harrison, L., Touizer, E., Peacock, T. P., Spencer, M., Zuliani-Alvarez, L., &
1131 Towers, G. J. (2019). Disrupting HIV-1 capsid formation causes cGAS sensing of viral DNA.
1132 *BioRxiv*, 838011. https://doi.org/10.1101/838011
1133 Takeda, E., Murakami, T., Matsuda, G., Murakami, H., Zako, T., Maeda, M., & Aida, Y. (2011).
1134 Nuclear exportin receptor cas regulates the NPI-1-mediated nuclear import of HIV-1 vpr. *PLoS*
1135 *ONE*. https://doi.org/10.1371/journal.pone.0027815
1136 Taylor, S. L., Frias-Staheli, N., Garcia-Sastre, A., & Schmaljohn, C. S. (2009). Hantaan Virus
1137 Nucleocapsid Protein Binds to Importin Proteins and Inhibits Tumor Necrosis Factor Alpha-
1138 Induced Activation of Nuclear Factor Kappa B. *Journal of Virology*, *83*(3), 1271–1279.
1139 https://doi.org/10.1128/jvi.00986-08
1140 Trotard, M., Tsopoulidis, N., Tibroni, N., Willemsen, J., Binder, M., Ruggieri, A., & Fackler, O. T.
1141 (2016). Sensing of hiv-1 infection in tzm-bl cells with reconstituted expression of sting. *Journal of*
1142 *Virology*, *90*(4), 2064–2076. https://doi.org/10.1128/JVI.02966-15
1143 Vermeire, J., Naessens, E., Vanderstraeten, H., Landi, A., Iannucci, V., van Nuffel, A., Taghon, T.,
1144 Pizzato, M., & Verhasselt, B. (2012). Quantification of Reverse Transcriptase Activity by Real-
1145 Time PCR as a Fast and Accurate Method for Titration of HIV, Lenti- and Retroviral Vectors.
1146 *PLoS ONE*, *7*(12), e50859. https://doi.org/10.1371/journal.pone.0050859
1147 Vodicka, M. A., Koepp, D. M., Silver, P. A., & Emerman, M. (1998). HIV-1 Vpr interacts with the
1148 nuclear transport pathway to promote macrophage infection. *Genes and Development*, *12*(2),
1149 175–185. https://doi.org/10.1101/gad.12.2.175
1150 Wu, Y., Zhou, X., Barnes, C. O., DeLucia, M., Cohen, A. E., Gronenborn, A. M., Ahn, J., & Calero, G.
1151 (2016). The DDB1-DCAF1-Vpr-UNG2 crystal structure reveals how HIV-1 Vpr steers human
1152 UNG2 toward destruction. *Nature Structural and Molecular Biology*, *23*(10), 933–939.
1153 https://doi.org/10.1038/nsmb.3284
1154 Xu, S., Ducroux, A., Ponnurangam, A., Vieyres, G., Franz, S., Müsken, M., Zillinger, T., Malassa, A.,
1155 Ewald, E., Hornung, V., Barchet, W., Häussler, S., Pietschmann, T., & Goffinet, C. (2016).
1156 cGAS-Mediated Innate Immunity Spreads Intercellularly through HIV-1 Env-Induced Membrane
1157 Fusion Sites. *Cell Host and Microbe*, *20*(4), 443–457.
1158 https://doi.org/10.1016/j.chom.2016.09.003
1159 Xu, W., Edwards, M. R., Borek, D. M., Feagins, A. R., Mittal, A., Alinger, J. B., Berry, K. N., Yen, B.,
1160 Hamilton, J., Brett, T. J., Pappu, R. V., Leung, D. W., Basler, C. F., & Amarasinghe, G. K.
1161 (2014). Ebola virus VP24 targets a unique NLS binding site on karyopherin alpha 5 to selectively
1162 compete with nuclear import of phosphorylated STAT1. *Cell Host and Microbe*, *16*(2), 187–200.

1163 https://doi.org/10.1016/j.chom.2014.07.008
1164 Yan, J., Shun, M. C., Zhang, Y., Hao, C., & Skowronski, J. (2019). HIV-1 Vpr counteracts HLTF-
1165 mediated restriction of HIV-1 infection in T cells. *Proceedings of the National Academy of*
1166 *Sciences of the United States of America*, *116*(7), 9568–9577.
1167 https://doi.org/10.1073/pnas.1818401116
1168 Yan, N., Regalado-Magdos, A. D., Stiggelbout, B., Lee-Kirsch, M. A., & Lieberman, J. (2010). The
1169 cytosolic exonuclease TREX1 inhibits the innate immune response to human immunodeficiency
1170 virus type 1. *Nature Immunology*, *11*(11), 1005–1013. https://doi.org/10.1038/ni.1941
1171 Ye, J., Chen, Z., Li, Y., Zhao, Z., He, W., Zohaib, A., Song, Y., Deng, C., Zhang, B., Chen, H., & Cao,
1172 S. (2017). Japanese Encephalitis Virus NS5 Inhibits Type I Interferon (IFN) Production by
1173 Blocking the Nuclear Translocation of IFN Regulatory Factor 3 and NF-κB. *Journal of Virology*,
1174 *91*(8), e00039-17. https://doi.org/10.1128/jvi.00039-17
1175 Yoneyama, M., Suhara, W., Fukuhara, Y., Fukuda, M., Nishida, E., & Fujita, T. (1998). Direct
1176 triggering of the type I interferon system by virus infection: Activation of a transcription factor
1177 complex containing IRF-3 and CBP/p300. *EMBO Journal*, *17*(4), 1087–1095.
1178 https://doi.org/10.1093/emboj/17.4.1087
1179 Zander, K., Sherman, M. P., Tessmer, U., Bruns, K., Wray, V., Prechtel, A. T., Schubert, E., Henklein,
1180 P., Luban, J., Neidleman, J., Greene, W. C., & Schubert, U. (2003). Cyclophilin A Interacts with
1181 HIV-1 Vpr and Is Required for Its Functional Expression. *Journal of Biological Chemistry*,
1182 *278*(44), 43202–43213. https://doi.org/10.1074/jbc.M305414200
1183 Zhang, C., Shang, G., Gui, X., Zhang, X., Bai, X. chen, & Chen, Z. J. (2019). Structural basis of
1184 STING binding with and phosphorylation by TBK1. In *Nature* (pp. 567(7748):394-398).
1185 https://doi.org/10.1038/s41586-019-1000-2
1186 Zhang, F., & Bieniasz, P. D. (2019). HIV-1 Vpr induces cell cycle arrest and enhances viral gene
1187 expression by depleting CCDC137. *BioRxiv*, 2019.12.24.888230.
1188 https://doi.org/10.1101/2019.12.24.888230
1189 Zhang, S., Feng, Y., Narayan, O., & Zhao, L. J. (2001). Cytoplasmic retention of HIV-1 regulatory
1190 protein V pr by protein-protein interaction with a novel human cytoplasmic protein VprBP. *Gene*,
1191 *263*(1–2), 131–140. https://doi.org/10.1016/S0378-1119(00)00583-7
1192 Zhu, H., Jian, H., & Zhao, L. J. (2004). Identification of the 15FRFG domain in HIV-1 Gag p6 essential
1193 for Vpr packaging into the virion. *Retrovirology*, *1*(26), 343–398. https://doi.org/10.1186/1742-
1194 4690-1-26
1195 Zila, V., Müller, T. G., Laketa, V., Müller, B., & Kräusslich, H. G. (2019). Analysis of CA content and
1196 CPSF6 dependence of early HIV-1 replication complexes in SupT1-R5 cells. *MBio*, *10*(6),
1197 e02501-19. https://doi.org/10.1128/mBio.02501-19
1198 Zufferey, R., Nagy, D., Mandel, R. J., Naldini, L., & Trono, D. (1997). Multiply attenuated lentiviral
1199 vector achieves efficient gene delivery in vivo. *Nature Biotechnology*, *15*(9), 871–875.
1200 https://doi.org/10.1038/nbt0997-871
1201